Available online at www.sciencedirect.com
SCIENCE DIRECT®
Pergamon
Acta Materialia 51 (2003) 5907–5939
Acta MATERIALIA
www.actamat-journals.com

Recent advances and future directions in magnetic materials☆

D.C. Jiles *

Materials and Engineering Physics Division, Ames Laboratory, Iowa State University, Ames, IA 50011-3020, USA

Accepted 31 August 2003

Abstract

This paper reviews recent developments in four important categories of magnetic materials that are currently of topical interest: soft magnets, hard magnets, magnetomechanical and magnetoelectronic materials. For each category the various properties of prime interest are discussed, how these differ from one class to another, and how these properties can be controlled. Recent developments in materials are highlighted through the consideration of a few selected new magnetic materials which are at the leading edge of current research, including: amorphous magnetic fibers, nanocrystalline permanent magnet materials, ferromagnetic shape memory alloys and spintronic materials.

Keywords: Magnetic properties; Hard magnets; Magnetoresistance; Magnetostriction; Soft magnets

1. Introduction

1.1. Magnetic properties of materials

The magnetic properties of materials are measured from certain defined points and derivatives obtained from the variation of magnetization with magnetic field as shown in Fig. 1. Magnetic materials are broadly classified into two main groups with either hard or soft magnetic characteristics. Soft magnetic materials can be magnetized by relatively low-strength magnetic fields, and when the applied field is removed, they return to a state of relatively low residual magnetism. Soft magnetic materials typically exhibit coercivities values of approximately 400 A m^{-1} (5 Oe) to as low as 0.16 A m^{-1} (0.002 Oe). Soft magnetic behavior is important in any application involving a change in magnetic induction. Hard magnetic materials retain a large amount of residual magnetism after exposure to a magnetic field. These materials typically have coercivities, H_c, of 10 kA/m (125 Oe) to 1 MA/m (12 kOe). The materials at the high coercivity end of this range are known as permanent magnets. These materials are used principally to supply a magnetic field.

The magnetic properties of materials can be divided into two general categories: those that are structure sensitive and those that are structure insensitive. Structure insensitive refers to properties not markedly affected by changes in materials

* Tel.: +1-515-294-9685; fax: +1-515-294 8727.
☆ The Golden Jubilee Issue—Selected topics in Materials Science and Engineering: Past, Present and Future, edited by S. Suresh.

1359-6454/$30.00
doi:10.1016/j.actamat.2003.08.011

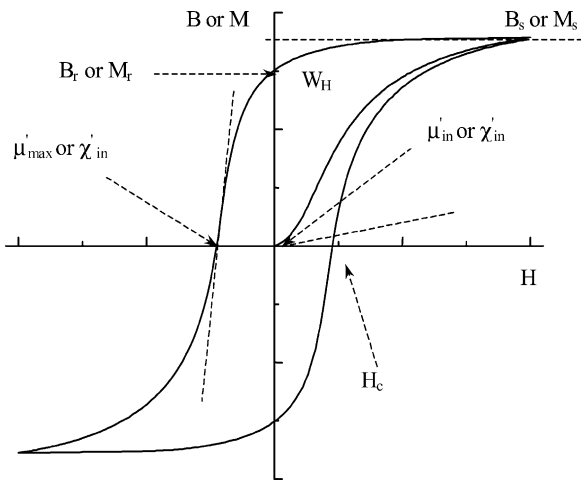

Fig. 1. Magnetic properties of materials as defined on the BH plane or flux density B versus magnetic field H, (or the MH plane of magnetization M versus magnetic field H). These include coercivity H_c, remanence B_R (M_R), hysteresis loss W_H, initial permeability μ_{in} (initial susceptibility χ_{in}), maximum differential permeability μ_{max} (maximum differential susceptibility χ_{in}) and saturation flux density B_s (saturation magnetization M_s).

processing (heat treatment or mechanical deformation) or by small changes in composition, including small amounts of certain impurities. Structure-insensitive properties include the saturation magnetization and resistivity. These properties are largely dependent on the composition of the particular alloy and are not changed substantially in the process of manufacturing a component from the alloy.

Structure-sensitive properties are those that are drastically affected by impurities. Small amounts of elements such as carbon, oxygen, nitrogen, and sulfur are commonly found in small quantities in magnetic materials. These elements tend to locate at interstitial sites in the crystalline lattice and consequently the lattice can be severely strained. As a result small concentrations of these elements can have large effects on some of the magnetic properties of the materials. Permeability, coercivity, hysteresis losses, remanence, and magnetic stability are all considered to be structure sensitive. The structure sensitive properties are controlled through processing of the material including mechanical and thermal treatments.

1.2. Units in magnetism

One can not go far in the subject of magnetism without encountering the problem of units, which is rather unique to this discipline. The reasons for this problem are hardly understood by those outside magnetism, but are a cause for continued controversy by the practitioners in the field. There are currently three main systems of units in widespread use in magnetism and several other systems of units which are variants of these. The three unit systems are the Gaussian or cgs system and two MKS unit systems, the Sommerfeld convention and the Kennelly convention. The basic units and equations of these three systems are summarized in Table 1. Each of these unit systems has certain advantages and disadvantages. The cgs and SI systems of magnetic units have different philosophies. The cgs system is based on an approach using magnetostatics and the concept of the ‘magnetic pole’, while the SI system takes an electrodynamic approach to magnetism based on electric currents. The SI system of units was adopted at the 11th General Congress on Weights and Measures (1960). The Sommerfeld convention was subsequently the one accepted for magnetic measurements by the International Union for Pure and Applied Physics (IUPAP).

2. Soft magnetic materials

Soft ferromagnetic materials are those magnetic materials with high permeability, low coercivity and low hysteresis loss [1, p. 600], which can be used to amplify the flux density generated by a magnetic field. The available range of magnetic properties of soft magnetic materials is continually being expanded. This amounts to reduction in coercivity, increase in permeability and consequently a decrease in hysteresis loss. Normally this can be accomplished through reduction in anisotropy and reduction in domain wall pinning. The latter can be strongly affected by the impurity content.

Table 1
Principal unit systems currently used in magnetism and the corresponding equations for flux density B, energy E and torque τ

Quantity		*SI (Sommerfeld)*	*SI (Kennelly)*	*EMU (Gaussian)*
Field	H	A/m	A/m	oersteds
Induction	B	tesla	tesla	gauss
Magnetization	M	A/m	-	emu/cc
Intensity of magnetization	I	-	tesla	-
Flux	Φ	weber	weber	maxwell
Moment	m	Am^2	weber metre	emu
Pole strength	p	Am	weber	emu/cm
Field equation		$B = \mu_0(H + M)$	$B = \mu_0 H + I$	$B = H + 4\pi M$
Energy of moment (in free space)		$E = -\mu_0 m \cdot H$	$E = -m \cdot H$	$E = -m \cdot H$
Torque on moment (in free space)		$\tau = \mu_0 m \times H$	$\tau = m \times H$	$\tau = m \times H$

Note: The intensity of magnetization I used in the Kennelly system of units is merely an alternative measure of the magnetization M, in which tesla is used instead of A/m. Under all circumstances therefore $I = \mu_0 M$.

2.1. Magnetic properties

2.1.1. Permeability

Permeability is the most important parameter for soft magnetic materials since it indicates how much magnetic induction B is generated by the material in a given magnetic field strength H. Initial permeabilities of all magnetic materials range from μ_r = 1,000,000 [1, p. 603] in materials such as amorphous alloys down to as low as μ_r = 1.1 in some of the permanent magnets. It is known that initial permeability and coercivity have in broad terms a reciprocal relationship, so that materials with high coercivity necessarily have a low initial permeability and vice versa.

2.1.2. Coercivity

Coercivity is the parameter which is used to distinguish hard and soft magnetic materials. Traditionally a material with a coercivity of less than 1000 A m^{-1} is considered magnetically 'soft'. A material with a coercivity of greater than 10,000 A m^{-1} is considered magnetically 'hard'. Low coercivities are achieved in nickel alloys such as permalloy in which the coercivity can be as low as 0.4 A m^{-1} [2].

2.1.3. Saturation magnetization

The highest saturation magnetization available in bulk magnetic materials is $M_s = 1.95 \times 10^6$ A/m (B_s = 2.43 T) which is achieved in an iron-cobalt alloy containing 35% cobalt. The possible values of saturation magnetization then range downward continuously to effectively zero. There has been little progress in improving the range of saturation magnetization of materials for about 100 years.

2.1.4. Hysteresis loss

The hysteresis loss is the area enclosed by the hysteresis loop on the B, H plane. It represents the energy expended per unit volume during one cycle of the hysteresis loop. The hysteresis loss increases as the maximum magnetic field reached during the cycle increases. This loss is closely related to the coercivity so that processing of materials to reduce coercivity also reduces the hysteresis loss. Generally low hysteresis loss is a desirable characteristic of soft magnetic materials.

2.1.5. Energy dissipation and power losses

A related property is the power loss which arises when a soft magnetic material is subjected to a time dependent magnetic field. The hysteresis loss is only one component of the power loss, being the

power loss obtained when the field is cycled very slowly under quasi-static conditions. The total power loss depends on the frequency of excitation, the amplitude of magnetic induction, the hysteresis loss, the physical dimensions of the material being magnetized and the eddy current dissipation. In addition there is usually a discrepancy between the measured power loss and the loss expected from the sum of hysteresis and eddy current losses and this is usually referred to as the "anomalous loss". The total electrical power loss can be expressed as the sum of these various components. Total power losses can be reduced if the conductivity of the material is reduced.

2.1.6. Barkhausen effect

The Barkhausen effect comprises a series of discontinuous changes in magnetization, sometimes known as 'Barkhausen jumps', that are caused by the sudden motion of domain walls or by the sudden rotation of magnetization within a domain. These can be observed along the magnetization curve provided sufficient resolution is used in measuring changes in flux density or magnetization.

2.2. New soft magnetic materials

2.2.1. Nanocrystalline magnetic materials

In recent years the range of available soft magnetic materials has been significantly increased by the development of nanocrystalline magnetic materials beginning with Yoshizawa et al. [3]. The materials are mostly based on iron alloys and have grain diameters of typically 10–15 nm. The exceptional properties of these materials, which have coercivities below 1 A m^{-1} (0.0125 Oe) and high relative permeabilities of typically 10^5 combined with relatively high saturation magnetization of $M_s = 1.05 \times 10^6$ A m^{-1} (13 kG) and resistivities as high as 1.15×10^6 ohm m. The most widely investigated alloy is $Fe_{73.5}Si_{13.5}B_9Nb_3Cu_1$, which is produced by rapid solidification and is then annealed above its crystallization temperature to produce the nanocrystalline structure. Developments in these nanocrystalline materials have been described by Herzer [4].

2.2.2. Artificially structured magnetic materials

Recent developments in soft magnetic materials have included what may be termed artificially structured materials in which the structure of heterogeneous materials is carefully controlled to produce the desired magnetic properties. A heterogeneous magnetic material consisting of nanocrystalline particles embedded in an amorphous magnetic matrix phase, as shown in Fig. 2, in which the magnetic properties of the particulate and matrix phases are essentially different, allows considerable scope for controlling the magnetic properties through structural changes brought about by annealing.

One example of this has been described by Hernando et at. [5], in which iron-silicon-boron nanocrystals are embedded in an amorphous matrix of the same material. This resulted in a material with a desirable low magnetic anisotropy, and hence low loss. The Curie temperature of the material, which is normally low for the amorphous alloys, can be controlled by the presence and size of the nanocrystalline particles. Curie temperatures in the range 200–350 °C can be obtained by annealing at different temperatures and for different times [6]. These are multiphase materials consisting of particulate and matrix materials with different magnetic and structural phases in which the eventual properties of the entire material can be controlled by structural changes to produce a material with

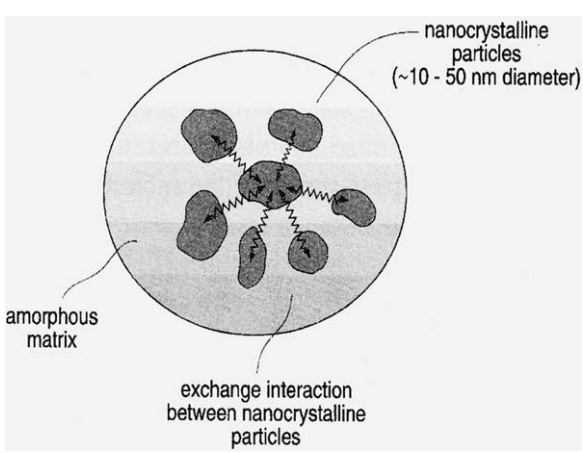

Fig. 2. Schematic of an artificially nanostructured magnetic material consisting of nanocrystalline particles embedded in an amorphous matrix, as described by Hernando et al. [5].

the desired combination of anisotropy and Curie temperature.

2.2.3. Amorphous magnetic ribbons

Soft magnetic alloys can be prepared in amorphous, noncrystalline form, known as metallic glasses. These have low anisotropy combined with high resistivity. As a result they have high permeability and low power losses. In the preferred planar-flow casting method of production, the metal is rapidly quenched from the melt onto cooled rotating drums to form long ribbons approximately 30–50 μm thick which can be up to 1 m wide. Those produced for soft magnetic materials are based on iron-, nickel-, and cobalt-alloys (and sometimes a combination of two of these magnetic elements). They also contain varying amounts of metalloids (boron, silicon, carbon, and phosphorus) which help to form the amorphous "glassy" phase, and other alloying elements such as chromium, molybdenum and aluminum.

These materials are characterized by low hysteresis loss and low coercive force. However, the Curie temperature is limited to approximately 475 °C and magnetic saturation is limited to approximately $M_s = 1.3 \times 10^6$ A m^{-1} (B_s = 1.7 T or 17 kG).

The low electrical conductivity of metallic glasses compared with crystalline soft magnetic materials, such as grain-oriented silicon steels, makes amorphous metals extremely attractive for reducing eddy current losses. The low coercive forces compared with competing crystalline materials also results in lower hysteresis loss in amorphous metals.

2.2.4. Amorphous magnetic fibers

One of the most important recent developments in soft magnetic materials has been amorphous magnetic fibers. Like the amorphous magnetic ribbons these are produced by rapid solidification from the melt, but in this case the material is ejected in a jet from a nozzle and quenched in a stream of liquid, usually water, but in some cases oil can be used for particularly reactive metals. The final product is a fiber or wire typically 50 μm in diameter which has no long range crystalline structure.

The compositions of amorphous magnetic fibers that have been most widely investigated are TM_x Si_y B_z, where TM is one of the transition metals Fe, Co or Ni. Typically x = 0.7–0.8, while y and z are each in the range 0.1–0.2. In some cases other transition metals are added such as Cr which improves the corrosion resistance. Fibers with positive magnetostriction based on Fe can be produced as well as fibers with negative magnetostriction based on Co. Those containing Co:Fe in the ratio of 16:1 result in an alloy with nearly zero magnetostriction.

Some of the early work on these amorphous magnetic fibers was by Ohnaka et al. [7] and by Mohri et al. [8]. The first application identified by Mohri for these materials was in 'jitterless' pulse generator elements, in which the sharp magnetization changes that occur in these materials over a wide range of frequency of applied field, are ideal. These rapid magnetization changes are due to large Barkhausen effect jumps inside the material which can be induced by field strengths as low as 10 A m^{-1} (0.12 Oe).

In most cases the amorphous fibers that have been produced and studied are iron-based materials, such as the $Fe_{81}Si_4B_{14}C_1$ composition. Other compositions based on the FeSiB glass-forming alloy include FeCoSiB, FeCrSiB and FeNiSiB as reported by Mohri et al. [9], who also suggested a domain model for the as-cast fibers which can explain the unusually large Barkhausen jumps in these materials.

Accordingly the basic model consists of an axially oriented 'core' domain running along the length of the fiber, surrounded by outer or 'shell' domains as shown in Fig. 3. The large Barkhausen jumps are caused by a sudden reorientation of the

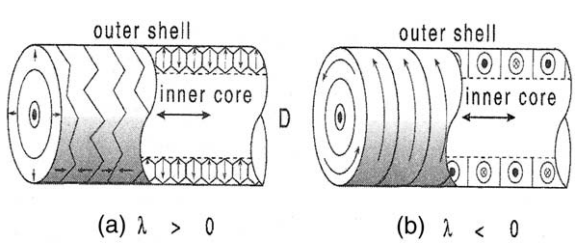

Fig. 3. Magnetic domain structures in amorphous wires with positive and negative magnetostrictions, after Mohri et al. [9].

core domain. The orientation of the 'shell' domains depends crucially on the magnetostriction of the material because the quenching process induces high levels of radial stress and hence stress-induced anisotropy in the radial direction. For materials with positive magnetostriction this results in radially directed magnetization in the 'shell' domains, whereas for materials with negative magnetostriction the 'shell' domains orient circumferentially.

The magnetic properties of these amorphous magnetic fibers are strongly affected by post-production heat treatment, as demonstrated by Atkinson et al. [10], in which FeSiB alloy fibers were studied. Annealing at 425 °C relieves the casting stresses in the fibers and results in an alteration of the ratio of core domain volume to shell domain volume. This has dramatic effects on the coercivity, remanence and field-induced magnetostriction. For example, the field-induced magnetostriction can be reduced by 50%, from 30×10^{-6} to 15×10^{-6}, by simply annealing the fibers for 600 s at 425 °C. The coercivity was also reduced from 7.0 to 2.9 A m^{-1} and the remanence ratio Mr/Ms was increased from 0.46 to 0.77.

Mohri et al. [11] have discussed the possible uses of the new amorphous magnetic wire materials. Many uses are directed principally towards sensors, which arises because of their high sensitivity of the magnetization to magnetic field, the rapid response and low power consumption/dissipation. The two main concepts are the giant magnetoimpedance effect (seen in amorphous wire materials with saturation magnetostriction $\lambda_s \sim 0$) and the stress impedance effect (seen in amorphous wire materials with $\lambda_s < 0$). The giant magnetoimpedance effect (GMI) in amorphous wires of FeCoSiB was first reported by Panina and Mohri [12]. Values of 60% were observed which was attributed to the skin effect and the strong field dependence of the circumferential permeability. This GMI effect is perhaps one of the most promising magnetotransport phenomena in new nanostructured magnetic materials.

Chiriac et al. [13] have studied saturation magnetostriction in amorphous wires and has developed nearly zero magnetostriction Co rich amorphous magnetic wires. Interest in the zero magnetostriction wires is high because of their almost reversible magnetization curves. They also studied the variation of saturation magnetostriction with stress which gave a derivative of $d\lambda/d\sigma = -0.9 \times 10^{-10}$ per MPa. Annealing of the material causes the sign of the saturation magnetostriction to change from -0.11×10^{-6} to $+0.3 \times 10^{-6}$. Change in the sign of magnetostriction causes dramatic changes in the domain structures because of the radially oriented tensile residual stress in the as-cast wires. This in combination with the magnetostriction determines the orientation of the outer shell domains, which results in differences in permeability and initial magnetization curves as shown in Fig. 4. Chiriac et al. [14] also investigated the magnetoelastic behavior in these Co-rich amorphous glass covered wires. In this the effects of iron content and stress annealing on magnetoelastic properties of the wires were studied. The main material of interest was $Co_{68}Fe_4Si_{13}B_{15}$ which has nearly zero magnetostriction. The magnetization data showed that the hysteresis loops of these materials are highly sensitive to stress, which offers excellent opportunities for the materials in stress sensors.

Chiriac and Ovari [15] also studied the GMI effect in families of soft magnetic wires as indicated in Fig. 5. It was found that magnetostriction of the materials plays a crucial role because in the absence of long range crystalline anisotropy there are very few factors, other than magnetoelastic and magnetostatic effects that determine magnetic properties. The circularly polarized shell domain structure is important in defining the properties. These circular domains exist at the surface of the $\lambda_s < 0$ amorphous wires. The result was wires with values of fractional change in impedance $\Delta Z/Z$ of 60%. The effects were found to be different in different "families" of wires.

Zhukova et al. [16] have investigated ways to maximize the giant magnetoimpedance in amorphous wires. A large sensitivity of up to $\Delta Z/Z = 300\%$ resulted from the application of a magnetic field. This can be explained in terms of the classical skin effect, using the model for the material that includes an outer shell of circumferential magnetization, and an inner core of axial magnetization as described previously by Mohri. In some of the

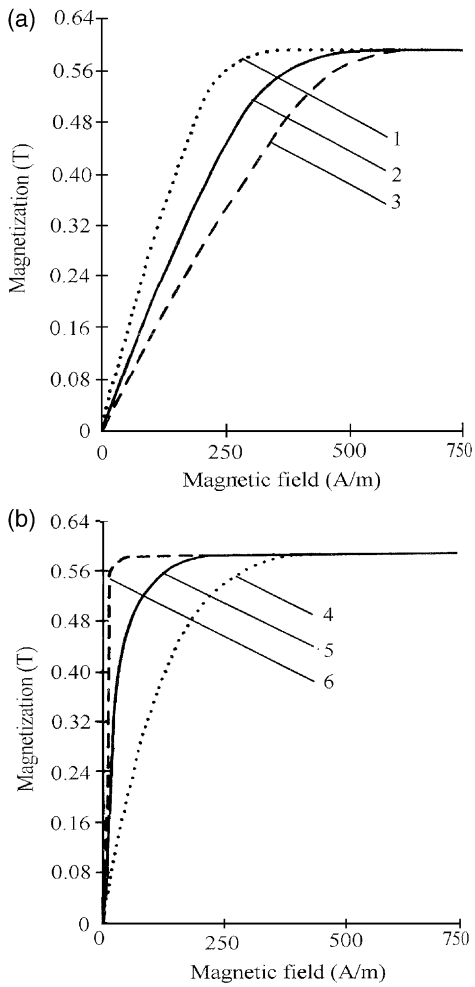

Fig. 4. Stress dependence of the magnetization curves in amorphous metal wires as described by Chiriac et al. [13]. The labels 1-6 refer to different tensile stress levels:- for 'as cast' material 1) α = 0, 2) α = 83, 3) α = 180 MPa, and for 'stress/current annealed' material 4) α = 0, 5) α = 83, 6) α = 180 MPa.

materials a magnetoimpedance of $\Delta Z/Z$ = 615% was reported.

Betancourt et al. [17] undertook theoretical studies to investigate a domain model for understanding the observed magnetoimpedance of amorphous magnetic wires. The material of most interest is 125 μm diameter amorphous wires of $Co_{68}Fe_4Si_{13}B_{15}$, with $\lambda_s < 0$ which has the circumferential shell domains. Betancourt performed calculations to determine the complex circular permeability of the wires from a model of inductance. Real components of inductance are associated with permeability while imaginary components are associated with dissipative processes. The complex circular permeability calculated in this way was in good agreement with experimental observations. Ciurenau et al. [18] has measured the circumferential and longitudinal permeabilities of Co rich amorphous wires at high frequencies up to the GHz range.

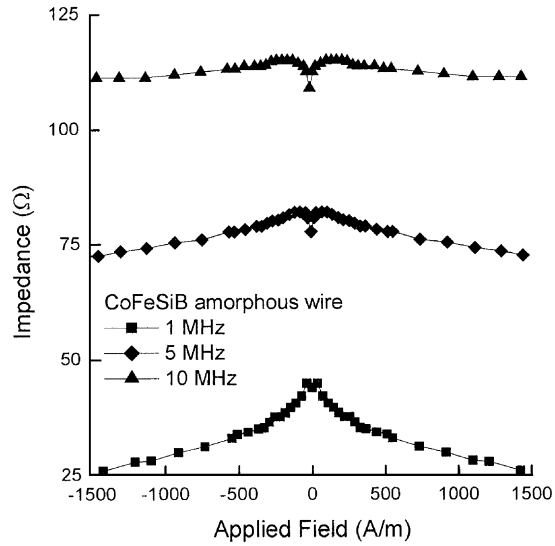

Fig. 5. Frequency dependence of the giant magnetoimpedance effect in amorphous magnetic wires, Chiriac and Ovari [15].

Li et al. [19] investigated GMI and magnetoelastic properties of stress annealed nanocrystalline FeCuNbSiB amorphous magnetic wires. The effects of stress annealing were studied using simultaneous applied stress and current. Values of $\Delta Z/Z$ of typically 150% were observed, as shown in Fig. 6. The behavior of the wires was explained in terms of a simple effective field model whereby the anisotropy of the material is altered by both annealing and stress which controlled the magnetic field at which the maximum in $\Delta Z/Z$ occurred. Zhukova et al. [20] has also shown the effects of stress on the magnetization and magnetic properties of FeSiB amorphous wires. The application of stress dramatically affects the magnetic properties of these materials because they have low anisotropy, but sufficiently high magnetostriction

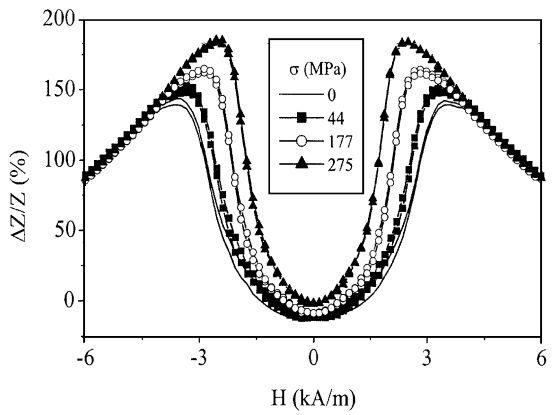

Fig. 6. Stress dependence of the giant magnetoimpedance (GMI) effect in nanocrystalline FeCuNbSiB magnetic wire after Li et al. [19].

which ensures that the magnetoelastic coupling strongly affects the easy direction of magnetization. They measured the effect of tensile stress on the hysteresis curves of these materials. The results can be understood in terms of two factors—magnetostatic and magnetoelastic energies. Magnetic remanence increased monotonically with tensile stress. Large Barkhausen jumps between two stable states were observed. They also studied the closure domain structure in the core. The slope of the hysteresis curves varied strongly with the length of the wires.

Losin et al. [21] have looked at the effects of torsional stress on the magnetic properties of amorphous magnetic wires. The material of principal interest was again $Co_{68}Fe_4Si_{13}B_{15}$. The torsional effect was measured showing that resistance and reactance of a circuit including these materials are only slightly affected by stress, whereas the second harmonic voltage amplitude and permeability are strongly affected by stress. Therefore GMI is itself not useful for stress detection, but on the other hand hysteresis or permeability measurements on the material are useful for stress detection.

Zhukov [22] have studied the magnetic properties of glass coated microwires. These wires had diameters of typically 100 μm and exhibited high sensitivity of the magnetic properties to stress. Because the magnetic properties of the zero magnetostriction materials were almost hysteresis free they have nearly reversible, one-to-one properties that may be useful for sensors. Some of the materials also showed large Barkhausen jumps and the giant magnetoimpedance (GMI) effect. Amorphous magnetic wire materials showing magnetic bistability can be useful for switches.

2.2.5. Other nanostructured soft magnetic materials

Kulik et al. [23] have also looked at magnetically soft nanostructured materials for high temperature applications; in this case amorphous ribbons consisting of nanocrystalline α-Fe/Co in an amorphous matrix. This was achieved by partial recrystallization of the material to form the nanocomposite. Addition of hafnium was found to inhibit crystal growth so that even after annealing for 700 hours at 500 °C the material was still nanocrystalline. The result was materials with coercivities of less than 50A/m.

In the search for new magnetic materials with different properties Fert and Piraux [24] investigated magnetic nanowires that were electrodeposited into the pores of membranes with 30–500 nm diameters. These were quite different in type from the amorphous soft magnetic wires investigated by Mohri, Chiriac and Hernando. They were multilayer wires, with coercivities in the range of hundreds of kA m^{-1} (~ a few kOe), which exhibited giant magnetoresistance of 15–25% depending on the temperature of measurement.

Petzold [25] investigated the properties of modern nanocrystalline soft magnetic ribbons for electronic device applications and these are compared with the magnetic properties of other soft magnetic materials in Fig. 7. The materials were produced from the rapidly solidified amorphous ribbons by a partial recrystallization anneal. The result was materials with a unique combination of low coercivity, high permeability and high thermal stability.

Amorphous magnetic materials provide a relatively simple model system for investigating domain wall motion. Himeno et al. [26] studied the dynamics of magnetic domain walls in amorphous magnetic wires and ribbons with an artificial constriction. The trilayer wires were prepared by electron beam lithography. The wires were similar to some of the layered structures that had already

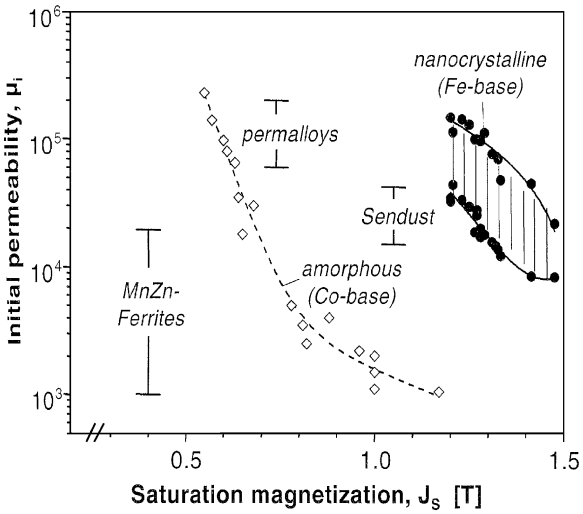

Fig. 7. Comparison of the initial permeabilities and saturation magnetizations of a variety of soft magnetic materials after Petzold [25].

been investigated for GMR in films and multilayers. The magnetization reversal process was studied using giant magnetoimpedance measurements. A constriction in the wire acted as a pining site for domain walls. Constriction widths of 0.25, 0.30 and 0.35 μm were studied and it was found that the strength of the required depinning field decreased with neck width. However the fractional change in resistance $\Delta R/R$ was found to be only 0.12%.

Moulin et al. [27] have studied nanocomposites of Fe and Fe/Ni dispersed in a Mn-Zn ferrite. The concept of a nanocomposite that can take advantage of the best properties of both materials. The simple idea here was to improve the saturation magnetization of the material by forming a nanostructured composite. A combination of nanostructured permalloy and ferrite gave a material with higher magnetization than the ferrites.

3. Hard magnetic materials

The term hard magnetic material is used to describe materials that have sufficiently high resistance to demagnetizing fields. Coercivity is therefore used to distinguish between hard and soft magnetic materials. The hard magnetic materials are classified as those with coercivities above 10 kA m^{-1} (125 Oe). The class of hard magnetic materials includes permanent magnets. The most recent permanent magnet materials have coercivities two orders of magnitude greater than this.

Permanent magnets are used for generating a magnetic field. The energy needed to maintain the magnetic field is stored when the permanent magnet is initially ‘charged’ (i.e. magnetized initially in a high field strength and then to remanence when the applied field is removed). Permanent magnet materials are based on the cooperation of a large number of magnetic moments within a magnet body to produce a high magnetic induction which is then retained because of a strong resistance to demagnetization, usually as a result of high anisotropy. Ferromagnetic elements such as iron and cobalt are widely used, and these are often alloyed with high anisotropy rare earth elements to produce high coercivity. Other elements, such as manganese or chromium, can be made ferromagnetic by alloying. Ferromagnetic metals combine with other metals or with oxides to form ferrimagnetic materials. Ceramic (“oxide”) magnets are of this type.

Permanent magnet materials are developed for their characteristic magnetic properties of: high remanent magnetic induction, high resistance to demagnetization, and high maximum energy product. Magnetic induction is limited by composition; the highest saturation induction is found in binary iron-cobalt alloys. Resistance to demagnetization is conditioned less by composition than by shape or crystal anisotropies and the mechanisms that subdivide materials into microscopic regions. Precipitations, strains and other material imperfections, and fine particle technology are all used to obtain a characteristic resistance to demagnetization.

Several different types of permanent magnet materials are now available and improvements in properties such as coercivity and maximum energy product continue to be made in rare earth transition metal permanent magnets and the development of two-phase ‘exchange spring’ magnets. The magnetization state of a permanent magnets is normally not deliberately changed. This need for stability of

output means that insensitivity to temperature effects, mechanical shock, and demagnetizing fields are important considerations in permanent magnets.

Permanent magnet materials include a variety of alloys, intermetallics, and ceramics. The most widely studied materials are: cobalt-rare earth alloys ($SmCo_5$ or Sm_2Co_{17}), and neodymium-iron-boron ($Nd_2Fe_{14}B$), iron-platinum, cobalt-platinum and hard ferrites (SrO-Fe_2O_3 or BaO-$6Fe_2O_3$).

3.1. Magnetic properties

When ferromagnetic materials are used as permanent magnets they must operate in conditions where they are subject to their own demagnetizing field and may even be subjected to various demagnetizing effects of magnetic fields in their vicinity. It is essential that they are not easily demagnetized. They must therefore have high coercivity, remanence and energy product. Maximum energy product is an important parameter because permanent magnets are used primarily to produce a magnetic flux density. Maximum energy content and certain other characteristics of materials used for permanent magnets, are best described by its hysteresis loop in the second quadrant which is sometimes referred to as the "demagnetizing curve".

3.1.1. Coercivity

The ability of permanent magnets to resist demagnetization is an important property and consequently a high coercivity is essential. Over the years there has been continual progress in the discovery of new permanent magnet materials with higher coercivities [28, p. 7]. For example, the intrinsic coercivity of neodymium-iron-boron is typically 1.1 MA m^{-1} (14 kOe) and for samarium-cobalt it is typically 0.69 MA m^{-1} (8.7 k Oe). In permanent magnets the magnetization is not simply an approximately linear function of the flux density, unlike soft magnetic materials in which B is approximately equal to $\mu_o M$. This is because the values of magnetic field H used with permanent magnets are generally much larger than in soft magnetic materials. The result of this is that the coercivity can be defined as either the field at which the magnetization M is zero, the intrinsic coercivity ${}_M H_c$, or the field at which the magnetic flux density B in the material is zero ${}_B H_c$. These quantities have quite different values in hard magnetic materials, and the greater the difference the better the material is as a permanent magnet. It should be noted that ${}_M H_c$ is always greater than ${}_B H_c$.

3.1.2. Remanence

In order to act as a source of magnetic field a permanent magnet is only of use if it has a relatively high magnetization when removed from an applied magnetic field. Therefore a high remanence is essential and this inevitably means a high saturation magnetization. The remanence M_R (or B_R) is the maximum residual magnetization (or magnetic flux density) that can be obtained in a closed-loop configuration in which there is no demagnetizing field. Since, to be of any use, all permanent magnets must be operated in an 'open circuit' configuration, the residual magnetization, or flux density, at which the permanent magnet operates in open circuit will always be below the remanence value. Therefore a combination of high remanence and high coercivity is essential to permanent magnets. The remanence in some of the most recent high performance $Nd_2Fe_{14}B$ is for example typically $M_R = 1.2 \times 10^6$ A m^{-1} ($B_R = 1.5$ Tesla) [29] and for Sm_2Co_{17} it is $M_R = 0.72$ A m^{-1} ($B_R = 0.9$ Tesla) [30].

3.1.3. Saturation magnetization

The remanence is of course dependent on the saturation magnetization, and for this reason the saturation magnetization of a permanent magnet should be large. While this condition is necessary it is not sufficient, since the squareness ratio M_R/M_S must also be as close to 1 as possible in order to ensure a large remanence. The saturation magnetization in neodymium-iron-boron is $M_S = 1.27 \times 10^6$ A m^{-1} ($B_S = 1.6$ Tesla) and in samarium-cobalt it is $M_S = 0.99 \times 10^6$ A m^{-1} ($B_S = 1.24$ Tesla) [31].

3.1.4. Maximum energy product

One parameter that is often of interest to specify the performance characteristic of a permanent magnet is the maximum energy product, which is

the maximum value of *BH* obtained in the second quadrant. This is closely related to the total hysteresis loss or area enclosed by the hysteresis loop. The interest of researchers in the maximum energy product of permanent magnets stems from the total energy associated with a permanent magnet. The maximum energy product is simply a measure of the maximum amount of useful work that a permanent magnet is capable of doing outside the magnet. There have been continual improvements in the maximum energy product of various permanent magnet materials, from tungsten steel to rare earth transition metal alloys, over the last hundred years, as indicated in Fig. 8. The highest values of BH_{max} have been obtained in neodymium-iron-boron permanent magnets [32,33]. The maximum energy product is often given in alternative non-SI units of MegaGauss-Oersted (MGOe). The conversion factors between MGOe, J m^{-3} and ergs/cc are as follows: 1 MGOe = 7.96 kJ m^{-3} = 79.6 Kerg/cc.

3.1.5. Demagnetization curve

The maximum energy product only gives limited information about the properties of a permanent magnet. A more useful way of displaying the magnetic properties of a permanent magnet is to plot the portion of the hysteresis loop in the second quadrant from the remanence point to the coercivity. This demagnetization curve indicates the magnetization under various demagnetizing fields. Such a curve contains information about the maximum energy product. The strength of the demagnetizing field of a permanent magnet in open-circuit configuration depends on the shape of the permanent magnet. Therefore the performance of permanent magnet material as a field source is dependent as much on the geometry as on the intrinsic material properties.

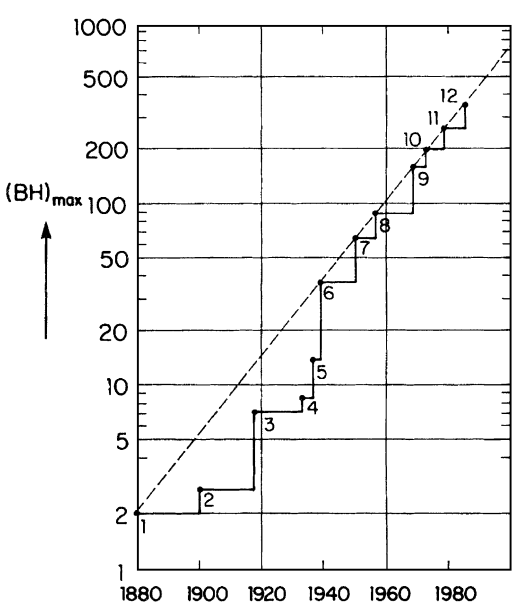

Fig. 8. Progress in the maximum energy product in permanent magnet materials [2, p.367].

3.2. New hard magnetic materials

3.2.1. Rare earth transition metal permanent magnets

Rare Earth Transition Metal (RETM) permanent magnets, based either on neodymium-iron-boron or samarium-cobalt alloys, have been the main focus of attention in hard magnetic materials in recent years. One of the disadvantages of $Nd_2Fe_{14}B$ is its rather low remanent magnetization in the isotropic form of the material. This is about $M_R = 0.64 \times 10^6$ A m^{-1} (0.8 T) compared with 1.05×10^6 A m^{-1} (1.3 T) in the anisotropic or oriented form of the material. The resultant energy product is 100 kJ m^{-3} (12.5 MG Oe) compared with 320–400 kJ m^{-3} (40–50 MG Oe) in some of the oriented material. In a theoretical paper Kneller and Hawig [34] proposed an idea for improving both the saturation and remanent magnetizations in permanent magnet materials by using a two-phase nanostructured material consisting of a magnetically hard phase embedded in a high saturation magnetically soft matrix. Such a material allows good exchange coupling between the two phases so that the high magnetization of the matrix phase helps to maintain a high magnetization in the hard phase. This idea became known as the ‘exchange spring’ magnet. An interesting prediction was that permanent magnet nanocomposites could be formed in this way consisting of 90% soft phase (such as α-Fe) and only 10% hard phase (such as $Nd_2Fe_{14}B$).

It was found experimentally that a structure of fine and regularly dispersed particles with grain size typically 10 nm does lead to enhanced M_S and M_R. Hadjipanayis et al. [35,36] were able to pro-

duce isotropic remanence enhanced magnets based on these ideas. The material consisted of a fine-grained composite of $Nd_2Fe_{14}B$ in a matrix of α-Fe which comprised 50–70 wt% of the material. The remanence ratios M_R/M_S in these materials improved from 0.5–0.78, although the coercivity was much reduced, 320 kA m^{-1} (4 kOe) compared with 1.2×10^6 A m^{-1} (15 kOe) in the normal neodymium-iron-boron material. Davies [37] has also reported that remanence enhancements from 0.8–1.2 T are achieved in NdFeB/α-Fe nanocomposites with grain sizes below 40 nm.

The exchange coupling between the hard and soft phases becomes relatively more important as the ratio of interfacial area to volume of the grains increases. While the intrinsic coercivity of these materials is lower than in normal NdFeB, the presence of the α-Fe on an ultrafine scale apparently does not result in serious deterioration of the maximum energy product, which remains at about 160 kJ m^{-3} (20 MGOe), a level comparable with NdFeB. These "remanence enhanced" magnets have received much attention and the idea has been extended to other materials. Ding, McCormick and Street [38] have reported large remanence enhancements in SmFeN using a nanocomposite with an α-Fe matrix.

Theoretical modeling by Schrefl [39] has shown excellent agreement with experimental results, confirming that the proposed mechanism is the reason for the enhancement in the properties. These calculations provided some of the most advanced materials property modeling for establishing a direct relationship between magnetic properties and the structure of the material.

3.2.2. Nanophase magnets based on rare earth transition metal alloys

Hadjipanayis [40] has considered various aspects of "nanophase hard magnets". These are nanocomposite magnets consisting of a very fine nanoscale mixture of exchange coupled hard and soft phases. As is generally known coercivity increases as particle size is reduced, reaching a maximum at the single domain size, thereafter decreasing to zero at the superparamagnetic limit, as shown in Fig. 9. The properties also depend strongly on whether the demagnetization process

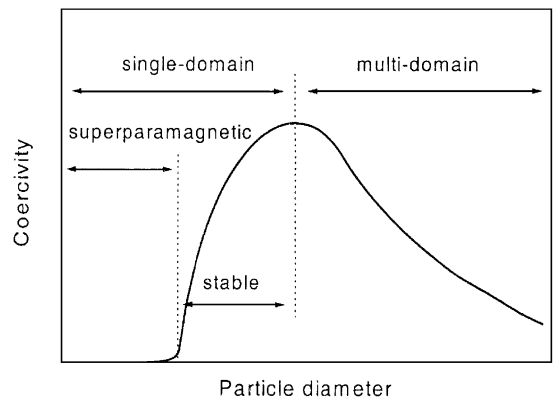

Fig. 9. Dependence of magnetic coercivity on particle size in permanent magnet materials as described by Hadjipanayis [40].

is principally via a nucleation mechanism or via a domain wall pinning mechanism, as indicated for an example of each in Fig. 10. In exchange coupled magnets an attempt is made to get the best of both types of materials that comprise the structure. They give higher B_R than the hard phase, and a higher H_c than the soft phase. This only applies if the phases consist of volumes that are small enough to be exchange coupled. Therefore particle size is a critical factor. Certain trade offs can be made to tailor

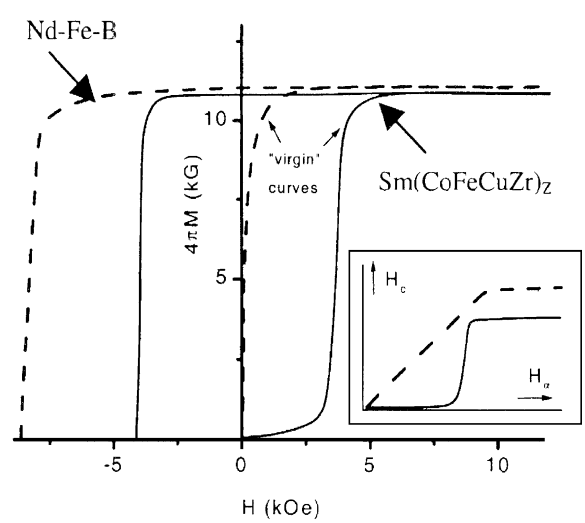

Fig. 10. Initial magnetization and demagnetization curves, and field amplitude dependence of coercivity (inset) in pinning type (eg. Sm2(CoFeCuZr)17) and nucleation type (eg.Nd2Fe14B) magnets, after Hadjipanayis [40].

the properties of the materials, since a larger fraction of magnetically hard material gives higher coercivity, whereas a larger fraction of soft gives higher remanence. The future direction of hard magnetic materials is towards structures with very fine particle sizes and a regular distribution of particles with uniform sizes.

Stamps [41] has investigated the mechanism of exchange bias in hard magnets in which he focused on magnetic thin film interfaces and spin electronics. Exchange bias is a phenomenon closely associated with magnetization and hysteresis in ferromagnetic/antiferromagnetic bilayers. The interactions between the antiferro- and ferro-magnetic phases are of great current theoretical interest, since the magnetic properties of the ferromagnetic film can be controlled by the presence of a nearby antiferromagnetic layer without the need for a magnetostatic field. Biased hysteresis loops result from the exchange coupling. It was found that the rate dependent magnetization processes are determined by thermal fluctuations in the material strong enough to unpin domain walls.

Skomski et al. [42] investigated exchange in permanent magnets propagated through a non-magnetic insulating matrix. In these cases the embedding of single domain magnetic particles in paramagnetic matrix should allow the coercivity to approach anisotropy field $H = 2K/\mu_o$Ms. The exchange coupling decreases exponentially with a characteristic decay length, which does not exceed several interatomic spacings. The characteristic decay length is affected by the nature of the matrix so that unless the matrix is close to ferromagnetic the decay length will be even shorter and is at most a few atomic spacings. If the interactomic spacing increases a strong decrease in exchange energy occurs. The small characteristic decay length, ~0.1 nm, emphasizes the relative weakness of interatomic (long range ordering) interactions compared with intra-atomic interactions.

Gutfleisch et al. [43] have considered nanocrystalline RETM permanent magnets. In these materials it is the grain size and the intergranular phases that combine to give properties that are different from bulk materials. Single domain particles give the highest H_c values and for most RETM permanent magnet materials the single domain size is <1 μm. In situations where there is an excess of rare earth metal beyond the stoichiometric composition (for example $Nd_2Fe_{14}B$) the rare earth rich material on the grain boundaries results in hard magnetic grains separated by paramagnetic layers and this gives high coercivity while stoichiometirc material $RE_2Fe_{14}B$ results in a single phase with exchange coupled grains. On the other hand rare earth deficient material gives $RE_2Fe_{14}B$ grains coupled through Fe_3B or other iron rich phases such as α-Fe in which the results can be materials with remanences higher than those expected on the basis of the Stoner-Wohlfarth model. Increasing (BH)max in this way can give 85% of the theoretical maximum for NdFeB magnets. Nevertheless coercivity values rarely exceed 30% of the anisotropy field.

Chiriac et al. [44] have also investigated glassy hard magnets based on NdFeAl. These were produced as amorphous ribbons with thickness ~150 μm and cast rods of the same material, with diameters <2 mm. The amorphous NdFeAl and NdFeSi ternary alloy systems can be produced in a wide range of compositions. Although structurally these can be formed as glasses, their magnetic properties are more characteristic of granular materials It was found that the coercivity could be increased to 0.6 MA/m at 200 K, as shown in Fig. 11, in a structure which consisted of a packing of nanometer sized clusters. The high coercivities of these alloys of NdFeAl result from the formation of small metastable or non-equilibrium magnetic clusters. Results are similar to those obtained on rare earth-iron binary amorphous alloys but different from those obtained on materials such as NdFeB in which the presence of the amorphous phase leads to soft magnetic characteristics.

Rodewald et al. [45] have investigated NdFeB sintered magnets with a minimization of RE rich constituents giving a very fine grained structure. These were subjected to pulsed field treatment to align the particles, resulting in a BHmax of greater than 56 MGOe Property values were: $Br = 1.5$ Tesla, (15 KG) ${}_MH_c = 7.8$ KA/m (9.8 KOe), and $BH_{max} = 451$ KJ/m^3 (56.7 MGOe).

Wang et al. [46] have studied the effects of Pr content on amorphous Pr(FeCo)B alloys. Exchange enhanced remanence and energy product obtained

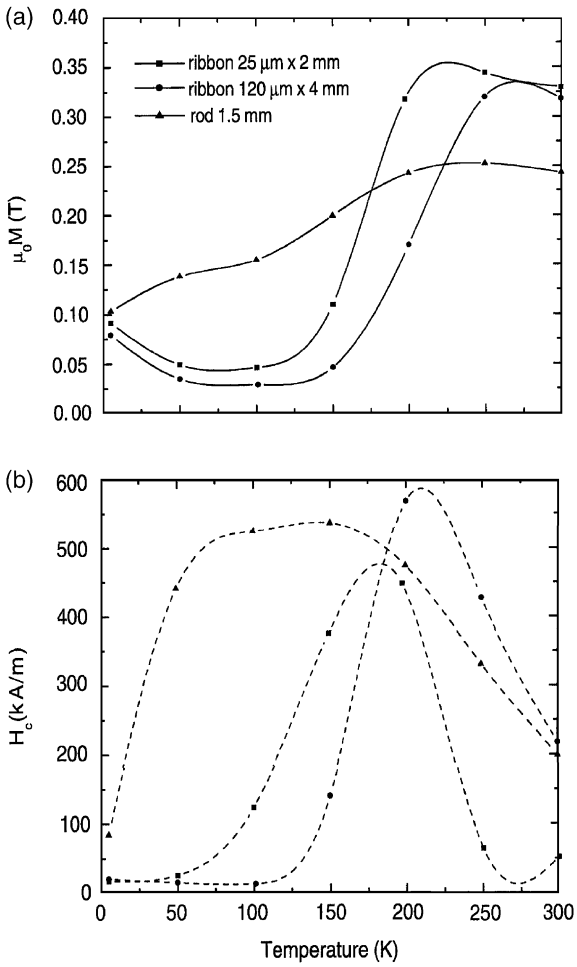

Fig. 11. Temperature dependence of the magnetization (upper figure) and coercivity (lower figure) of $Nd_{50}Fe_{40}Al_{10}$ amorphous alloy, after Chiriac et al. [44].

in nanocomposites of this alloy gave higher coercivity than the corresponding NdFeB alloys due to higher anisotropy. Annealing of the alloys gave high H_c (755 kA/m) and BH max (160 KJ/m^3), but this was obtained only for high Pr contents. For sub-stoichiometric alloys annealing caused deterioration of the hard magnetic properties. However T_c was lower for the Pr alloy than the Nd alloy.

Zhou et al. [47] reported on the effects of structure chemical composition and mechanical alloying on the magnetic hysteresis in SmCo nanocrystalline powders. A room temperature coercivity of 41 kOe was observed in Sm_2Co_7 compound. In samarium cobalt permanent magnets larger coercivity and enhancement of remanence can be achieved through control of grain size. Effects of the addition of Cu to the SmCo alloys were studied. Coercivity was found to increase with Cu content. In addition mechanical alloying and mechanical milling lead to improvements in hard magnetic properties.

Betancourt and Valenzuela [48] investigated enhanced coercivity in REFeAl based alloys. The specific alloys studied were NdFeAl and PrFeAl alloys, with small amounts of B, Cu, Dy added. These alloys are of interest because of the simple fabrication and processing. Coercivity in these alloys is attributed to short range order within the amorphous materials in which the structure actually consisted of an amorphous matrix with a small volume of fraction of hcp Nd crystallites embedded in the matrix. Coercivity was enhanced by the addition of either B, Cu or Dy. This is attributed mostly to domain wall pinning on the crystallites, but also to a lesser extent to alteration in the nucleation sites. The maximum coercivity obtained was 388 KA/m.

Branagan et al. [49] studied high hysteresis in a homogeneous TbAl metallic glass. The material produced was completely amorphous. Intrinsic coercivity approached 23 kOe and BH_{max} was 12.4 MGOe. The domain size in this glass was much larger than the structural cluster size. The high H_c was explained on the basis of exchange bias. No identifiable nuclei or second phases present. After crystallization the hard magnetic properties deteriorated, as shown in Fig. 12. A three phase structure formed, containing both hard and soft phases resulting in a wasp-waisted hysteresis loop and associated poor hard magnetic properties.

Wang et al. [50] have looked at the effect of Co substitution on $(PrTb)_2$ $(FeNbZr)_{14}B$ alloys. This alloy, which is of the "2–14–1" type, gives an indication of how complicated the situation is becoming in the search for new and improved permanent magnet materials as more chemical additions are being tried to enhance the range of properties. The Curie temperatures of the rare earth transition metal alloys sometimes precludes their use in certain applications. Therefore a search for permanent magnets with higher Curie temperatures has been

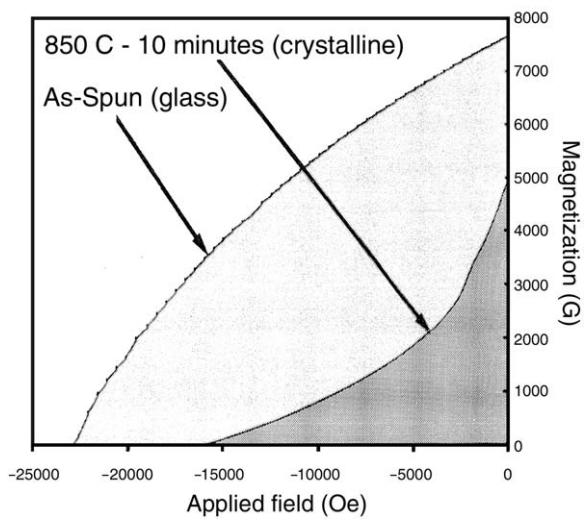

Fig. 12. Differences in the demagnetization curve of as spun and crystalline (heat treated) $Tb_{60}Al_{40}$ alloy after Branagan et al. [49].

undertaken. Nanocomposites were formed of both $RE_2Fe_{14}B/Fe_3B$ and $RE_2Fe_{14}B/\alpha$-Fe by melt spinning. Addition of Co greatly enhances the Curie temperature, and in this case typically 30% of the Fe was replaced with Co, so that T_c was increased from 775C in the iron alloy to 950 °C in the Co substituted alloy. The highest coercivities obtained were 6.8 KOe, with a maximum energy product of BH_{max} = 11.8 MGOe.

Ono et al. [51] studied crystallization and magnetic properties of NdFeCoVB and α-Fe/ NdFeB nanocomposite hard magnetic ribbons. As the amorphous volume fraction increased the crystal grain size became smaller and hard magnetic properties improved. An optimum quenching rate was found however which indicates that short range order is useful in order to inhibit grain growth of α-Fe crystals. The completely amorphous state was found to be less conducive to hard magnetic properties than one with a small volume fraction of nanocrystalline clusters containing Nd.

3.2.3. Nanophase magnets based on cobalt or iron and platinum

CoPt and FePt have emerged as candidates for high performance exchange spring magnets with enhanced magnetic properties. Both the CoPt and FePt materials have high anisotropies (4.9×10^6 J/m^3 and 6.6×10^6 J/m^3 respectively). The FePt system has the advantage of complete solid solubility at higher temperatures. At lower temperatures the crystal structure transforms from fcc to a face centered tetragonal structure which has improved hard magnetic properties due to the increased anisotropy.

Huang et al. [52] have studied hysteresis in CoPt nanoparticles embedded in a non-magnetic matrix consisting of C and/or BN. The effects of the particle size on properties were investigated. Thin films of these materials were prepared by sputtering. It was found that coercivity depended principally on the particle size. Annealing time and temperature were used to produce optimum particle sizes. Whereas the "as-fabricated" films had $H_c <$ 8 kA/m (100 Oe), annealing caused an increase in particle size and a consequent increase in H_c from less than 80 KA m^{-1} (1 kOe) to 1000 KA m^{-1} (12 kOe).

Barmak et al. [53] investigated ferromagnetic exchange spring nanocomposite films. These consisted of CoPt films 10–25 nm thick, produced by dc magnetron sputtering. Various annealing treatments were used subsequently. The magnetic properties of the material changed from nucleation dominated behavior at low volume fractions of magnetically hard phase, to pinning dominated behavior at high volume fractions of hard phase. The particle size in the films increased with annealing time, resulting in increased coercivity. The reason was that the coercivity mechanism becomes increasingly pinning controlled as the volume fraction of the high coercivity phase increases. Even though the films were in all cases two phase structures the properties exhibited what was described in the paper as "single phase" magnetization behavior at all stages, meaning that there were no obvious macroscopic discontinuities in the magnetization curves that could be indicative of second phases.

Crew and Stamps [54] have described ferromagnetic resonance in exchange coupled thin films via theoretical calculations, using the micromagnetic Landau-Lifschitz-Gilbert model. For the experimental part of the magnetic resonance study Co/CoPt exchange coupled thin films were made.

It is known that the resonance frequency is determined in part by the perpendicular anisotropy in the film, and that such measurements can be used to find the perpendicular anisotropy. However exchange coupling between the films caused significant changes in the resonant frequency. It was also shown that magnetostatics plays an important role in determining the behavior.

Zhou et al. [55] have investigated improvements in the properties of FePt through exchange coupled FePt–Fe layered films prepared by magnetron sputtering, In FePt thin films a maximum energy product of up to BH_{max} = 15 MGOe, and in CoPt thin films a maximum energy product of up to BH_{max} = 50 MGOe were observed as shown in Fig. 13. The fabrication process produced exchange coupled FePt–Fe multilayers and it was found that in combination with a rapid thermal anneal an improved energy product of 19 MGOe could be obtained in these multilayers.

Thang et al. [56] also investigated magnetic properties of FePt alloys, in this case with Nb and/or Al doping. They studied the combined effects of annealing and the presence of third elements on the magnetic properties of these alloys. The materials consisted of exchange coupled grains, with domain sizes of typically 1–20 nm. A high coercivity resulted principally from pinning of domain walls. In the Al doped materials the observed magnetic properties were: BH_{max} = 120 KJ/m^3, H_c = 300 KA/m, B_r =1.025 Tesla (10.25 KG, $M_r = 0.82 \times 10^6$ A m^{-1}). The Nb doped material had similar properties except for a lower remanence of B_r = 0.975 Tesla (9.75 KG, $M_r = 0.78 \times 10^6$ A m^{-1})

Huang et al. [57] investigated fabrication and magnetic properties of FePt/C films containing FePt nanoparticles in order to increase the coercivity compared with the normal FePt thin films. The films were produced with FePt particle sizes in the range 3–20 nm. For the films with the smallest particle sizes the blocking temperature, which marks the boundary between hysteretic and non-hysteretic behavior, was found to be 200 K as shown in Fig. 14. For films with larger particles sizes the blocking temperature is higher. Once the particle sizes were such that the blocking temperature was above room temperature it was found that the coercivities were greater for the films with larger particles. A coercivity of 1.84×10^6 A m^{-1} (23 kOe) was obtained for the 8 nm diameter particles and a coercivity of 2.72×10^6 A m^{-1} (34 kOe) for the 15 nm diameter particles. It was also found that by depositing FePt simultaneously with carbon the structure of the films can be controlled so that strong perpendicular anisotropy can be produced in the films, suitable for magnetic recording media applications.

Ding et al. [58] have looked at phase transformation in FePt nanoparticles. As is known the material transforms from fcc to face centered tetragonal with high anisotropy and for this reason the

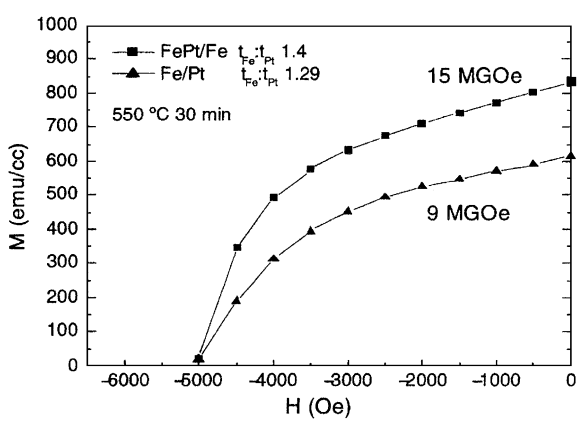

Fig. 13. Demagnetization curves of annealed FePt single layer film, and annealed FePt/Fe multilayer film after Zhou et al. [54].

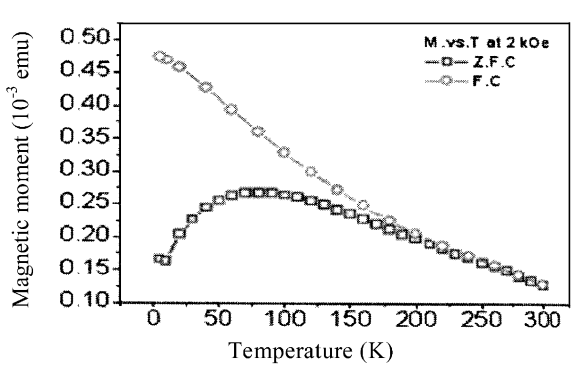

Fig. 14. Dependence of magnetization on temperature for field cooled (F.C.) under 2 KOe (160 KA/m) applied field and zero field cooled (Z.F.C) nanoparticles of $Fe_{50}Pt_{50}$ alloy, after Huang et al. [57].

material has potential for use in ultra-high density recording media applications. However annealing to cause the desired phase transformation is usually accompanied by sintering of the material which degrades the magnetic properties. Different annealing conditions were tried in order to get the best magnetic properties by achieving the phase transformation without the unwanted sintering. It was found that particle coalescence occurred at about 550 °C and once started proceeded very rapidly. Since this is also the temperature what which the phase transformation occurs it remains problematic. One solution that was suggested was to alloy the FePt with some other elements to try to reduce the transformation temperature below the sintering temperature—or alternatively to increase the particle separation in the film.

Simizu et al. [59] have also investigated exchange coupling in FePt magnets, the properties of which are given in Table 2. Those alloys in the range $Fe_{40}Pt_{60}$ to $Fe_{60}Pt_{40}$ alloys, exhibit the phase transformation from fcc to face centered tetragonal. Both phases can coexist, so this leads to the prospect of an exchange coupled magnet consisting of one material in two different structural and magnetic phases. The alloy $Fe_{60}Pt_{40}$ has a (BH)max of 120 KJ/m^3 (15 MGOe) and high squareness ratio of $M_r/M_s = 0.68$, a value which is consistent with that predicted in the exchange coupled model. This enhanced remanence was shown not to be due to texturing of the material, since magnetization curves were identical in three orthogonal directions. Also it was found that the "as quenched" samples had the hardest magnetic properties, and any annealing procedure that was attempted in order to promote formation of the hard magnetic phase was found to reduce H_c and B_r. Paradoxically therefore the best hard magnetic properties were obtained by suppressing the formation of the hard phase.

4. Magnetomechanical materials

These are materials in which the strong magnetomechanical coupling causes strain in the material when magnetized. The class of magnetomechanical materials is rather broad, but includes magnetoelastic materials in which the recovery of strain is reversible when the field is removed, and other materials for which the induced strain does not necessarily recover simply on removal of the magnetic field. These latter materials could be called magneto-plastic materials, but are often described as magnetic shape memory alloys. High performance magnetomechanical materials include cobalt ferrite, iron-gallium alloys, rare earth metals such as dysprosium and terbium, rare earth-iron alloys such as Terfenol (terbium-dysprosium-iron), and shape memory alloys such as NiMnGa and GdSiGe.

4.1. Magnetic properties

4.1.1. Magnetostriction

Magnetostriction is the fractional change length of a material when magnetized, either spontaneously by virtue of a magnetic phase transition (spontaneous magnetostriction) or under the action of a magnetic field (field induced

Table 2
Energy product, remanence, saturation, remanence to saturation ratio, and coercivity of three samples (x, y and z) of 'as cast' material and two heat-treated samples (16 hours at 600 °C and 16 hours at 650 °C) of $Fe_{0.6}Pt_{0.4}$

$Fe_{0.6}$ $Pt_{0.4}$	As cast			16 h/600 °C	16 h/650 °C
	x	y	z	z	z
BH_{max} (MG Oe)	4.87	5.33	5.94	5.36	4.15
B_r (kG)	6.86	7.34	7.63	7.13	6.49
B_s (kG)	10.37	10.92	11.20	10.60	10.36
B_r/B_s	0.66	0.67	0.68	0.67	0.63
H_c (kOe)	2.37	2.34	2.36	2.40	2.11

magnetostriction). The magnetostriction λ is the fractional change in length under the action of a magnetic field

$$\lambda = \left(\frac{\Delta \ell}{\ell_o}\right) \tag{1}$$

where ℓ_o is the original length and $\Delta\ell$ is the change in length. For convenience the length ℓ_o is usually taken as the length in the demagnetized state and the changes are therefore measured by convention relative to the demagnetized state. This effect is only significant in magnetically ordered materials such as ferromagnets, ferrimagnets and antiferromagnets. Typical magnetostrictive strains of magnetic materials are of the order of $\ell \approx 10^{-5}-10^{-6}$, [60] although more recent advanced materials, such as terbium dysprosium iron, have magnetostrictions as high as 10^{-3} [61,62].

4.1.2. Motor coefficient (strain derivative)

The strain derivative $d\lambda/dH$ for magnetostrictive materials, d, is a useful representation of materials properties, since it indicates how rapidly the strain changes with the relevant applied field,

$$d = \left(\frac{d\lambda}{dH}\right)_\sigma \tag{2}$$

This is also sometimes known as the strain coefficient, strain derivative, or simply as the "d coefficient". When changes expressed by differentials are small and reversible this d coefficient is also equal to $(dB/d\sigma)_H$ where B is the magnetic flux density and σ is the stress. It is a useful measure of the performance of a material, since it is closely related to the energy conversion efficiency of the material. However the dependence strain on magnetic field is also hysteretic. It is often quoted in the range of nanometers per amp in magnetostrictive materials. Typical values of the d coefficient for various materials are: $CoO.Fe_2O_3$ ~1×10^{-9} m A^{-1}, $Gd_5Si_2Ge_2$, ~1×10^{-9}m A^{-1}, Fe ~0.3×10^{-9} m A^{-1}, Ni ~-2×10^{-9} m A^{-1}, Co ~-0.2×10^{-9} m A^{-1}, polycrystalline $(Tb_{0.3}Dy_{0.7})Fe_2$ ~1.3×10^{-9} m A^{-1}.

4.1.3. Generator coefficient

When a magnetic material generates a change in magnetic field by application of a stress the parameter of interest is the rate of change of H field with stress, $dH/d\sigma$. This is called the generator coefficient g since it generates a field from applied stress at constant magnetic flux density

$$g = -\left(\frac{dH}{d\sigma}\right)_B = \left(\frac{dM}{d\sigma}\right)_B \tag{3}$$

This is measured in units of $AN^{-1}m$. It is also equal to the derivative of the magnetization M with respect to stress at constant magnetic flux density B as given in the equation. When the changes represented by the differentials are small and reversible this g coefficient is also equal to $-(d\lambda/dB)_\sigma$.

4.1.4. Coupling coefficient

An important consideration in magnetomechanical materials is often the efficiency for converting one form of energy into another (eg. mechanical into magnetic or vice versa). The input energy is usually supplied by an external influence such as an applied stress or a magnetic field. The response of the material, is in the form of strain or magnetization.

The energy conversion efficiency can be expressed via the square of the coupling coefficient, k which is defined as k^2 = (energy output)/(energy input). In the case of a magnetostrictive material k^2 is related to the materials properties by the equation

$$k^2 = \frac{E_Y}{\mu_o \mu_r} d^2 \tag{4}$$

where E_Y is the appropriate elastic modulus, μ_r is the relative permeability, μ_o is the permeability of free space and d is the d coefficient given by Eq. (2) above. However it must be remembered that in ferromagnetic materials μ_r is not constant. This means that the energy conversion efficiency changes with applied field strength.

4.1.5. Piezomagnetism

Under certain conditions the application of stress to a magnetic material can cause a change in magnetization. Only a few examples are known of

magnetic materials which can change from a demagnetized to a magnetized state under the action of a stress. One of these is the antiferromagnet CoF_2 in which a small magnetization of the order of 10^3 A/m can be produced by large shear stresses [63]. There are no known cases of ferromagnets which become magnetized under the action of a stress on the unmagnetized state. A related and much more common phenomenon is the tendency of magnetic materials to change their magnetization under the action of an applied stress when already magnetized [64]. This effect is only of significant size in ferromagnets and ferrimagnets. Jiles [65], and later Li and Jiles [66] have studied these effects. In these phenomena the order of application of stress and magnetic field is critical. The effects of change in stress on the magnetization have been modeled. The hysteretic nature of the behavior dictates that simple linear differential equations based on the "small amplitude" Maxwell relations are not valid for describing these effects.

4.2. New magnetomechanical materials

4.2.1. Gaint magnetostrictive rare earth transition metal alloys

Much progress has been made in recent years in the development of giant magnetostrictive materials such as Terfenol-D ($Tb_xDy_{1-x}Fe_2$ with $x \sim 0.3$). Reliable model descriptions of these materials have been developed at the same time, and these can now provide valuable predictive simulations of materials properties and performance. Calkins, Smith and Flatau [67] have developed a magnetostrictive model based on energy considerations which gave good agreement with performance of Terfenol-D. The model described the B, H hysteresis loop of the material, and then incorporated a non-hysteretic quadratic relationship between magnetostriction and magnetization. In this way a hysteretic relationship between magnetostrictive strain and applied magnetic field was obtained. The model was able to describe strain under both major and minor loop excursions of magnetization versus magnetic field. The model is also compact because it has only a small number of model parameters and can be operated under a wide variety of conditions including non-linear regimes.

Dapino, Smith and Flatau [68] have shown how to include non-linear and hysteretic effects directly into the description of strain. In this case, both the elastic compliance and the piezomagnetic coefficient d were allowed to be variable and path dependent. This generalization of the magnetostrictive model is suitable for describing the behavior of magnetostrictive materials at high fields.

4.2.2. Magnetic shape memory alloys

Shape memory alloys can exhibit deformations of 5–10% on application of a magnetic field. Ullakko et al. [69] were first to report unusually large magnetically induced strains in ferromagnetic shape memory alloys based on the Heusler alloy composition. Ni_2MnGa is a member of the family of Heusler alloys which undergoes a thermomechanical martensitic phase transformation on cooling below $T_m = 202$ K. Since the ferromagnetic transition is at $T_c = 376$ K the structural transformation occurs while the material is in its ferromagnetic state. Both transition temperatures T_m and T_c are sensitive to the chemical composition. Substitution of Mn for Ni can cause T_m to increase and T_c to decrease. These two temperatures coincide for compositions of $x \sim 0.18$–0.20 in $Ni_{2+x}Mn_{1-x}Ga$, according to Vassiliev [70], whereupon it transforms from a high temperature paramagnetic phase to a low temperature ferromagnetic phase simultaneously with the structural transformation from high temperature cubic to low temperature tetragonal. The c/a ratio is 0.94, which gives rise to a 6% deformation.

The martensitic transition can also be induced by a magnetic field. The application of a magnetic field leads to a redistribution of the structural state of the material. In order to obtain a colossal deformation under the action of a magnetic field the following criteria have been identified: i) the transition has to be thermoelastic, ii) the martensitic phase must be ferromagnetic iii) the martensitic phase must have sufficient anisotropy.

Sozinov et al. [71] have investigated crystal structures and magnetic anisotropy of Ni_2MnGa with giant field induced strain. In this study non-stoichiometric alloys were investigated. It was

found that, depending on the exact details of the crystal structure, a 6–10% strain can be induced by an applied field of less than 1 Tesla.

Pasquale et al. [72] have also studied magnetic and mechanical properties of Ni_2MnGa single crystals. Large field induced strains were produced in oriented single crystals by pre-treating the materials by subjecting them to a sequence of mechanical cycles and thermal treatments. Typical treatment needed to "stabilize" the samples involved a load of 20 MPa and a thermal treatment of 200 °C. Stress and field were applied subsequently. A repeatable sequence of "pseudoplastic" behavior was obtained which gave a 1.2% irreversible strain under a field of 450 kA/m (5.6 kOe) with an equivalent stress value of 12.5 MPa. The "pseudoplastic" region is defined as that where the strain changes with no additional stress due to the induced phase transformation, as shown in Fig. 15.

Khovailo et al. [73] studied the entropy change at the martensitic transformation in Ni_2MnGa. They investigated ΔS between the high temperature cubic phase and the low temperature tetragonal phase. The lowest value of ΔS was obtained for the stoichiometric alloy composition. Thereafter, as shown in Fig. 16, ΔS was found to increase with increasing nickel content beyond the stoichiometric composition. This is presumably due to an increase in the magnetic contribution to the entropy change.

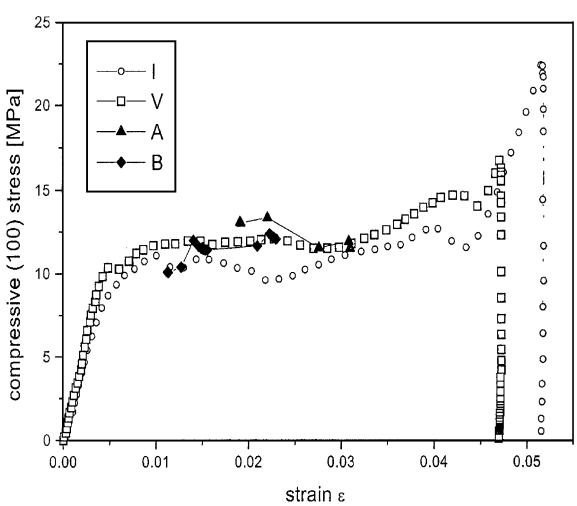

Fig. 15. Compressive stress v. compressive strain curves at 20C for Ni_2MnGa after Pasquale et al. [72] showing the pseudo plastic regime once the stress exceeded12 MPa (unfilled circles and unfilled squares). The filled triangles and filled diamonds show portions of the stress-strain curve obtained dduring magnetomechaincal characterization, in which the sample was subjected to a 20MPa load, aan anneal at 200C and then a restoration of the load to 12 MPa.

4.2.3. Magnetostructural phase transformation alloys

Samolyuk and Antropov [74] studied the magnetostructural phase transformation in $Gd_5(Si_{1-x}Ge_x)_4$. They investigated the stability of the magnetic structures theoretically. They showed that the effective Heisenberg exchange interaction decreased with deformation. This decrease in exchange coupling gave rise to the first order magnetostructural phase transition.

Casanova et al. [75] investigated the change in entropy at the first order magnetoelastic phase transition in $Gd_5(Si_{1-x}Ge_x)_4$. This was performed using differential scanning calorimetry under the simultaneous action of a magnetic field. It was shown that the variation of M with both field H and temperature T in each phase outside the immediate "phase transition region" gave an additional change in entropy to add to that observed during the transition.

Han et al. [76] have looked at the effects of sample purity on the thermal expansion of polycrystal-

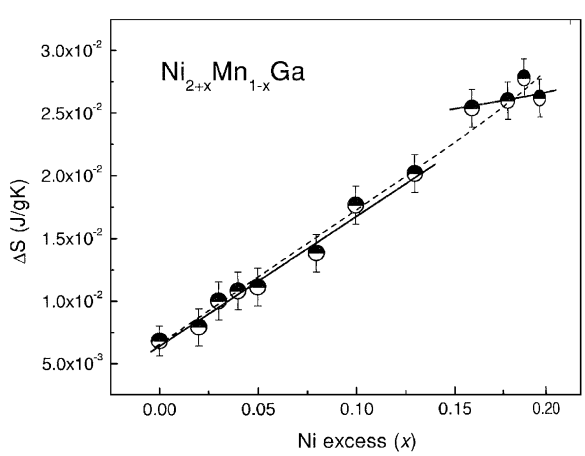

Fig. 16. Entropy change ΔS at the martensitic phase transformation in $Ni_{2+x}Mn_{1-x}Ga$ shape memory alloy as a function of the nickel content, after Khovailo et al. [73].

line $Gd_5(Si_{1-x}Ge_x)_4$ at the magnetostructural phase transformation temperature of 270 K. Measurements were taken on two samples made from different purity gadolinium. Thermal expansion results confirmed the existence of a first order phase transition with a discontinuity of 8000 ppm in the curve of strain versus temperature at the Curie point. It was found that the Curie temperature was lower for the lower purity sample, but the strain was larger in the lower purity material.

Han et al. [77] have also looked at the magnetoelastic properties of single crystal $Gd_5(Si_{1-x}Ge_x)_4$ alloys. The order-disorder transition can be induced by either field or temperature. Measurements were made for the first time of thermal expansion on single crystal specimens. Results showed a hysteresis in T_c of about 2 degrees depending on whether the temperature was being increased or decreased, as shown in Fig. 17. Results also showed an unusual field dependence of the transition temperature indicated in Fig. 18. Jiles et al. [78] have also looked at extraordinary magnetoelastic coupling in single crystal specimens of these $Gd_5(Si_{1-x}Ge_x)_4$ materials. The effects of application of a magnetic field on the Curie point transition temperature was demonstrated and the transition temperature was found to be linearly dependent on the magnetic field with a derivative of about 5K/T.

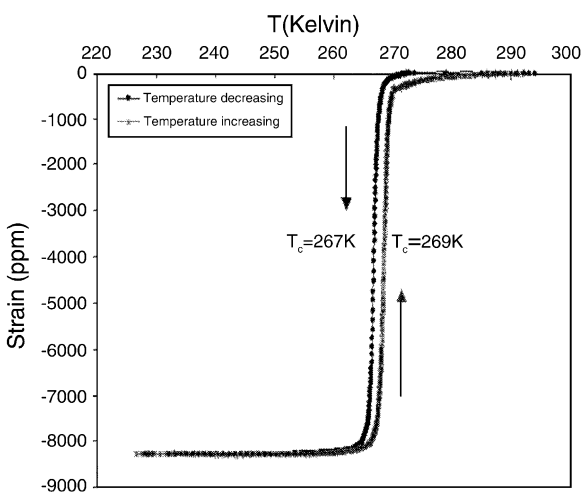

Fig. 17. Hysteresis in the Curie temperature of $Gd_5Si_2Ge_2$ as seen from thermal expansion measurements, after Jiles et al. [78].

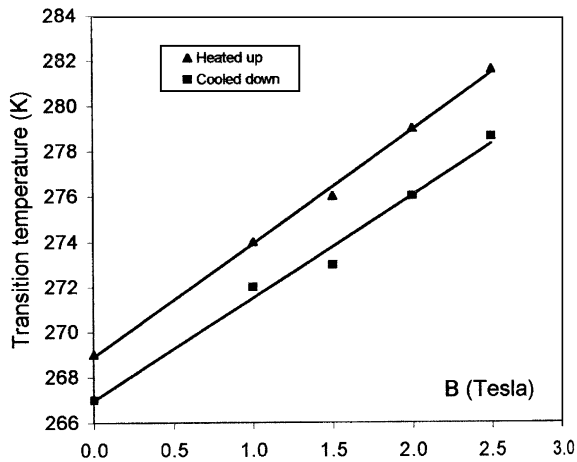

Fig. 18. Unusual dependence of the Curie temperature on applied magnetic field in $Gd_5Si_2Ge_2$, after Jiles et al. [78].

Han et al. [79] have found another surprising result in this material concerning the field dependence of the Curie temperature. It was shown that T_c is different when the magnetic field is applied along different crystallographic axes and the difference in the values of T_c along the different directions depends on the field strength.

4.2.4. Iron gallium alloys

Clark et al. [80] investigated extraordinary magnetoelasticity and lattice softening in bulk, single crystal bcc Fe–Ga alloys. Both Al and Ga have high solid solubility in Fe. As the Ga content is increased the material retains the local bcc structure and the saturation magnetostriction increases. The single crystal magnetostriction coefficient λ_{100} exhibited two peaks as the Ga content was increased, showing 265×10^{-6} at 19% Ga and 235×10^{-6} at 27% Ga as indicated in Fig. 19. The other single crystal magnetostriction coefficient λ_{111} was found to be much smaller than λ_{100}. and therefore did not play a significant role in the composition dependent behavior of the bulk magnetostriction. The variation of the magnetostriction as a function of Ga content was interpreted in terms of the variation of the magnetoelastic coupling coefficient b_1 and a strongly temperature dependent shear modu-

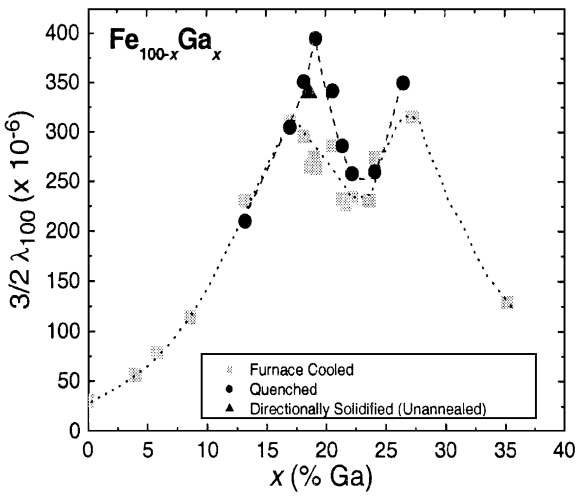

Fig. 19. Variation of the magnetostriction of $Fe_{100-x}Ga_x$ alloys with composition x as described by Clark et al. [80].

lus c_{11}–c_{12}. Surprisingly the magnetoelastic coefficient b_1 showed only one peak as the Ga concentration increased.

Cheng et al. [81] has also investigated the structure and properties of melt spun FeGa magnetostrictive materials with different alloy compositions. The objective of the investigation was to try to retain the disordered phase at higher Ga compositions by melt spinning of the alloy. Alloys of the type $Fe_{1-x}Ga_x$ in the range ($x = 0.17$, 0.21, 0.25, 0.3) were rapidly quenched to form ribbons. It was found that the Curie temperature T_c of $Fe_{79}Ga_{21}$ was 681 °C with saturation magnetostriction of λ_s = 98 ppm, whereas the T_c of $Fe_{83}Ga_{17}$ was 715 °C and λ_s = 130 ppm. Magnetostriction was measured along the ribbon length. The addition of Ga to iron increases λ_{100} from 20×10^{-6} to 207×10^{-6} at a composition of Ga ~ 17–19%. Above this concentration a structural change occurs in the material and the value of magnetostriction decreases.

Kellogg et al. [82] studied the dependence of saturation magnetostriction on texture and grain morphology in polycrystalline $Fe_{83}Ga_{17}$. The FeGa alloys exhibit magnetostrictive strains of >100 ppm in polycrystalline form whereas for [100] oriented materials the bulk strain can be up to 300 ppm. Control of crystallographic texture can be achieved through rolling deformation in order to maximize the resulting magnetostrictive strain. However the results of the measurements disagreed with the predictions of finite element model calculations (37 ppm was observed, whereas 157 ppm was predicted).

5. Magnetoelectronic materials

Magnetic materials can be used in information technology either as the medium for storing the data or as the sensors needed for detecting the magnetized regions on the medium. To make this of any practical use it must be possible to store large amounts of data in as small a space as possible. Consequently there is a drive to improve data storage densities, and currently these are doubling in less than a year. The ultimate goal is to establish fully integrated spintronics in which the devices that are selected for their magnetic functions are an integral part of the structure instead of an "add on" needed to achieve the desired functionality. Once this is achieved a new class of magnetoelectronic/spintronic materials and devices [83] will emerge which will offer a range of enhanced possibilities, including the prospect of all metallic transistors with very high charge carrier densities as a replacement for semiconductor transistors, and significant improvements in data storage densities.

5.1. Magnetic properties

5.1.1. Hysteresis: saturation, remanence and coercivity

The hysteresis of magnetization versus magnetic field in ferromagnets and ferrimagnets can be used for data storage. As a result of hysteresis the remanent magnetization of the medium acts as a memory of the last field maximum. Therefore data, either in digital or analog form can be stored as magnetic 'imprints' on magnetic media. The requirements are that the magnetic material must have high saturation magnetization to give as large a signal as possible. The coercivity must be sufficient to prevent unanticipated erasure, but small enough to allow the local regions for the material material to be easily remagnetized when necessary. Coercivities in the range of 20–100 kA m^{-1} are

common for magnetic recording media, although in the future in order to continue to improve storage densities the coercivity of the media will need to increase further. Therefore materials with coercivities in the range 200–240 kA m^{-1} (2.5–3 kOe) will be used [84]. For magnetic materials used in read and write heads the requirements are different. These materials have soft magnetic property requirements to allow the magnetic flux density in the read head or the write head to be as high as possible for a given field strength. Therfore permeability should be as high as possible, while coercivity and remanence should be as low as possible.

5.1.2. Magnetoresistance

The electrical resistance of some magnetic materials can change quite dramatically when a magnetic field is applied. Normally this effect is measured in terms of the fractional change in resistance $\Delta R/R$ versus magnetic field. In the case of materials such as permalloy $\Delta R/R$ can be about 2% at magnetic saturation.

Giant magnetoresistance (GMR) occurs in some multilayers when the relative orientations of the magnetic moments are changed. The change in resistance usually amounts to a decrease when a strong enough magnetic field is applied. If the magnetic moments in the successive layers are parallel the material has relatively low resistance, but when the moments are antiparallel the material has relatively high resistance. This is due to differences in the scattering of the electrons depending on which of the two polarizations they have, as explained below.

The first layered magnetic material to exhibit this ‘giant magnetoresistance’ was Fe/Cr/Fe [85], as shown in Fig. 20, and this was soon followed by other materials including Fe/Au/Fe [86], Co/Au/Co [87] and a range of other layered structures including Co/Cu/Co [88]. The magnitude of the effect depends on several factors including the thickness of the layers. The physical effect that causes this change in resistance with field is the spin-dependent scattering of electrons. This means that when moving between the magnetic layers electrons with spins in one direction are scattered more than electrons with spins in the other direction [89]. The band theory of magnetism provides an explanation

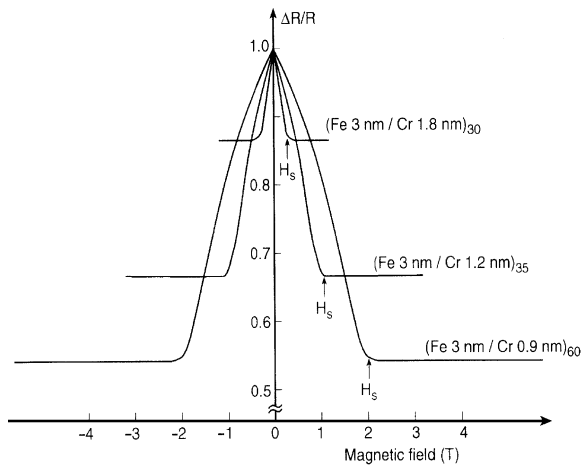

Fig. 20. Giant magnetoresistance ΔR/R in Fe/Cr/Fe multilayers of different thicknesses, showing up to 45% decrease in an field of 2 Tesla, after Baibich et al. [85].

of this effect as described by Fert et al. [90]. The change in resistance with change in relative orientation of the directions of magnetization in the successive magnetic layers can be attributed to the spin-dependent conduction of the electrons in these itinerant electron ferromagnets. The majority (“spin up”) and the minority (“spin down”) electrons have different densities of states and mobilities at any given energy due to the exchange splitting of the energy bands [91] as indicated in Fig. 21. Consequently the conductivities of these two groups of electrons can be different. Therefore electrons with a particular energy and spin orientation which pass from a layer where the magnetization, and hence the majority spins, are pointing to the right, to a layer where the magnetization, and hence the majority spins, are pointing to the left, experience a dramatic change in their conductivity.

In situations where the electron mean free path is larger than the thickness of the layers, in the antiparallel magnetization configuration all electrons which move across the layer boundaries find that they are strongly scattered in alternate layers, whereas in the parallel configuration one group of electrons will be weakly scattered in both magnetic layers, while the other group will be strongly scattered in both magnetic layers. The resistivity is

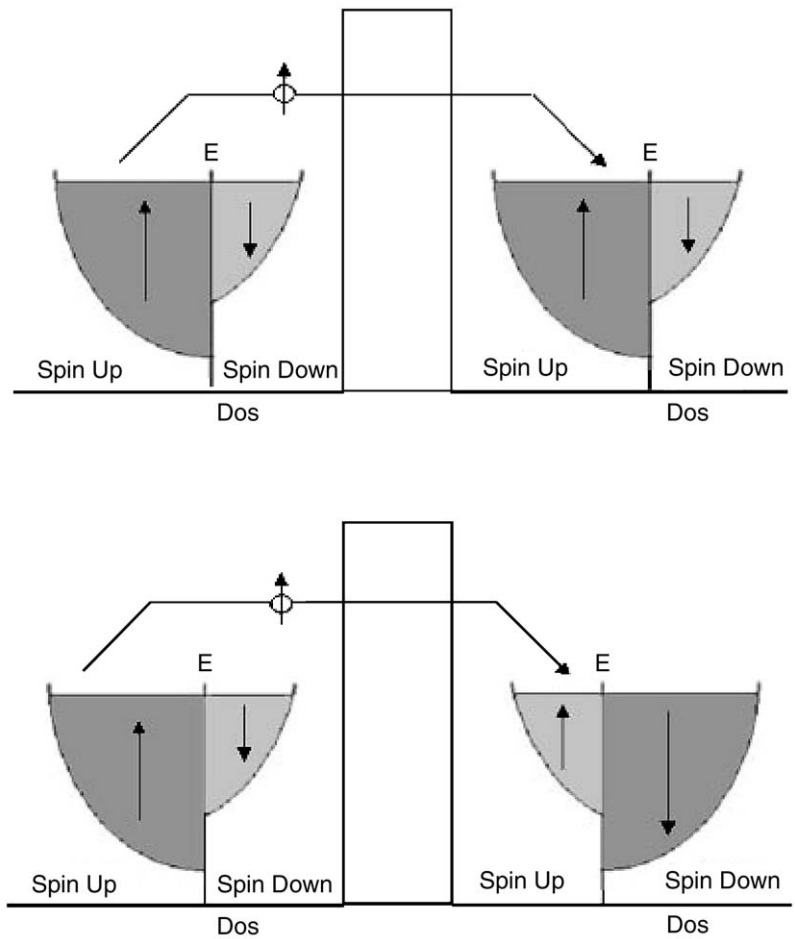

Fig. 21. Schematic of the electron band for a tunnel junction with the magnetizations in both electrodes parallel (upper figure) and antiparallel (lower figure), as described by Leib et al. [91].

therefore much lower in the parallel configuration than in the antiparallel configuration.

This change of resistance when subjected to a magnetic field can be used to develop high resolution sensors, such as read heads, which can detect the magnetic state of regions on the magnetic medium. Rapid progress in storage densities recently has been due principally to the development of giant magneto-resistive multilayers, which have led to the production of a new generation of high-sensitivity, high spatial resolution read heads [92]. These magnetic multilayers can exhibit changes in resistance $\Delta R/R$ of 80%.

The magnetoresistive material is used to detect the leakage flux from the locally magnetized regions of the recording medium by means of a two-point resistance measurement. To obtain an antisymmetric response that is approximately linear with strength of the leakage field, the magnetoresistive material also needs to be biased with another constant applied field. This is often supplied by using an adjacent magnetized film.

5.2. New magnetoelectronic materials

5.2.1. Magnetoresistive spin valves

GMR devices can be constructed in which one of the ferromagnetic layers is strongly pinned in a particular direction through exchange coupling to an additional nearby antiferromagnetic layer. In

this way an exchange biased magnetic electrode can be used to create what is known as a "spin valve" whereby the magnetization of one layer (the free layer) can be more easily oriented by application of a magnetic field than the magnetization of the other layer (the pinned layer). These materials have high magnetoresistance and low resistance that make them suitable for read head sensors.

The spin valves can employ either current in the plane "cip" or current perpendicular to the plane "cpp" configurations. Bass and Pratt [93] have discussed structures that employ current perpendicular to plane "cpp" magnetoresistance because the "cpp" magnetoresistance is usually larger than the "cip" magnetoresistance, as shown in Fig. 22, and many layered magnetoresistive structures can be operated in either mode. New directions of investigation for these materials include ballistic transport, in which the free path length of the electrons is greater than the dimensions of the device.

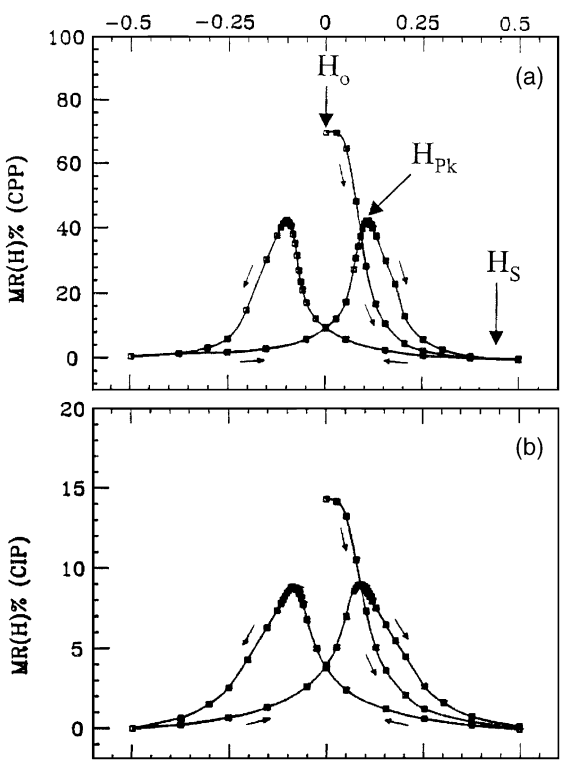

Fig. 22. CPP (upper figure) and CIP (lower figure) magnetoresistances for a Co/Ag/Co multilayer at 4.2 K after Bass and Pratt [93], showing that the cpp magnetoresistance is larger.

Generation and control of spin polarized currents in devices such as spin valves has been demonstrated in a metallic mesoscopic spin valve device by Jedema et al. [94] in which ferromagnetic electrodes of permalloy (Ni–Fe) were used to drive a spin polarized current into copper. This allows control of spin polarized currents in solid state devices at room temperature through the use of ferromagnetic contacts and marks a significant development towards "all metallic" electronic devices, such as diodes and transistors, as an alternative to conventional semiconductor devices. In these all-metallic spin valve structures the resistances are lower than in the tunnel junctions and the fractional change in resistance is about 10%. The all-metallic devices have the possibility of high storage densities, which are comparable to magnetic tunnel junctions. However because of the lower resistance of the all metallic structures they have low read out voltages. In addition a slow response time means longer read/write times of about 100 ns. Together these two factors have prevented them reaching performance levels that are acceptable for magnetic random access memory (MRAM) applications. Therefore these devices seem to have better prospects for sensors than for data storage.

Schumacher et al. [95] has investigated the precessional magnetization reversal in microscopic spin valve cells. The main interest is to enable rapid reversal of the magnetization in these structures. Possible uses in ultra fast, low power magnetic memory cells such as MRAM are envisaged where the data can be written rapidly. The rapid reversal of magnetization was achieved by the application of field pulses along the hard axis. Short, intense field pulses were applied with the direction oriented perpendicular to the initial magnetization direction of the domains. This resulted in stable and reversible switching of the magnetization direction with switching reliability greater than 99.8%.

Spin valves in which the pinned or free layer have been oxidized have shown enhancement of the magnetoresistance over conventional unoxidized spin valves as described by Veloso et al. [96].

A theoretical study of the anomalous magnetoresistance behavior of these oxidized spin valves using a modified Stoner-Wohlfarth approach, has been performed by Ventura et al. [97] to explain the behavior. In particular they investigated the field dependence of the magnetoresistance at different temperatures of CoFe spin valves consisting of a structure with MnIr/CoFe/nano-oxidized CoFe/CoFe/Cu/CoFe/Ta. They have extended the theoretical understanding of a spin valve by separating the pinned layer into two sublayers which are ferromagnetically coupled across an intermediate nano-oxide layer. The results showed that the behavior of these materials, including the anomalous behavior of the magnetoresistance at low temperatures, can be explained in terms of the strength of the ferromagnetic coupling between the upper and lower magnetic sublayers of the pinned layer, and the coupling between the antiferromagnetic MnIr layer and the bottom magnetic sublayer of the pinned layer, both of which control the reversal in magnetization of the pinned layer. Changing the applied field from the negative maximum at which parallel alignment occurs first causes the reversal of the pinned layer. This occurs gradually in stages because of the composite structure of the pinned layer, until high resistance antiparallel alignment has been established. As the field is increased to small positive field strengths the free layer suddenly switches from parallel to antiparallel configuration, resulting in a discontinuous reduction in magnetoresistance.

In order to improve the performance of spin valve devices Yuasa et al. [98] have studied the effect of inserted Cu on the current perpendicular to plane GMR in $Fe_{50}Co_{50}$ spin valves formed by deposition of multilayers of Cu and FeCo. The solid solubility of Cu in the $Fe_{50}Co_{50}$ magnetic electrode material is an important factor in increasing the spin dependent scattering. The result is that the change in resistance area product of the spin valve is enhanced by the use of the Cu layer, typically 5nm thick between the free and the pinned layers.

5.2.2. Magnetic tunnel junctions

These devices have similarities to spin valves and that most device designs are analogous to those using spin valves. These devices also use the current perpendicular to plane (cpp) configuration. The tunneling current that passes across the junction also differs depending on the relative orientations of the magnetization vectors in the two magnetic layers, as shown in Fig. 23. In magnetic tunnel junctions the magnetoresisitivities are higher than in GMR and spin valve devices, which is due to the use of an intermediate insulating layer instead of a metallic layer. These devices are useful for both data storage and sensors, in which their main characteristics are: large signal to noise ratios (sensors) and non-volatility (data storage).

Moodera et al. [99] developed the first magnetic tunnel junctions. Magnetic tunnel junctions in their simplest form consist of a three layer sandwich of two magnetic layers separated by a thin, 0.5–1.0 nm, non-magnetic, non-conducting layer. Moodera and Mathon [100] have reviewed spin polarized tunneling in ferromagnetic junctions. Tunneling magnetoresistance values of up to 30% have been achieved repeatably. Spin polarization $(n^{\uparrow}-n_{\downarrow})/(n^{\uparrow}+n_{\downarrow})$, where $n^{\uparrow}$ is the number density of "spin up" electrons and $n_{\downarrow}$ is the number density of "spin down" electrons, within the conduction band of the magnetic electrodes is an important factor in determining the tunneling magnetoresistance since this gives the direct measure of the excess popu-

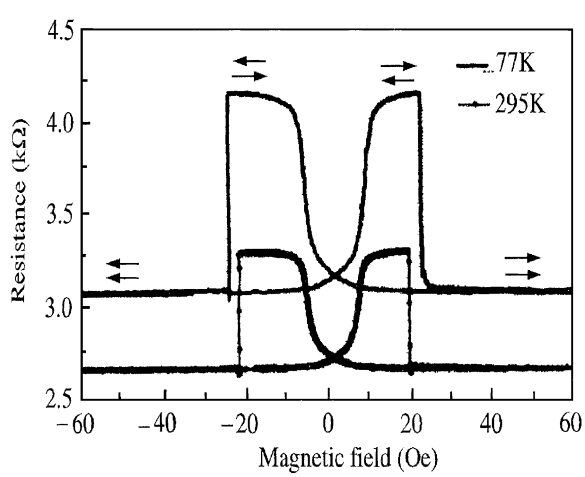

Fig. 23. Variation of resistance with magnetic field for a $Co/Al_2O_3/Ni_{80}Fe_{20}$ tunnel junction at room temperature 295K and at liquid nitrogen temperature 77 K, after Moodera and Mathon [100].

lation of one spin type over the other. This has a value of 50% in a material such as $Fe_{50}Co_{50}$.

Tunnel junctions have several attractive features including the possibility of fabricating MRAM with extremely high data storage densities [101]. Random access memories (RAM) that are currently in use for data storage in computers are based solely on semiconductor technology and therefore data that is stored in these memories is lost when the power supply is interrupted. On the other hand magnetic memories offer the prospect of non-volatile RAM whereby the magnetic states of the memory bits are not altered by the voltage interruptions and therefore data is preserved [102]. Prototype MRAM devices have already been shown to have improved on the speed and power consumption of conventional non-volatile semiconductor memory by several orders of magnitude, and have reached data storage densities and speeds that are comparable with those of conventional volatile dynamic RAM.

Reiss et al. [103] have reported on the properties and applications of magnetic tunnel junctions, in particular the strong dependence of tunneling current on external field at constant applied voltage. Device sizes that have been scaled down to below 0.01 mm^2 are of interest in order to achieve high data storage densities and high spatial resolution sensors. Considerations of single domain behavior, switching properties and edge coupling effects are important in trying to understand the behavior of the magnetization of the material at these length scales.

For MRAM type applications the most important consideration is a “clean” rapid reversal of magnetization. Size and aspect ratio of the devices play an important role in determining the switching field, as shown in Fig. 24. Warot et al. [104] have studied the magnetic properties of patterned tunnel junctions with a view to both MRAM and read head sensor applications. Magnetization reversal was studied using Lorentz microscopy. Several energy terms need to be considered in order to understand the properties. These include Neel coupling, stray field magnetostatic coupling and shape anisotropy. It was found that the high saturation magnetization in NiFeCo was principally responsible for the difference in behavior between tunnel junction fabricated with it and similar tunnel junction fabricated with NiFe free layers.

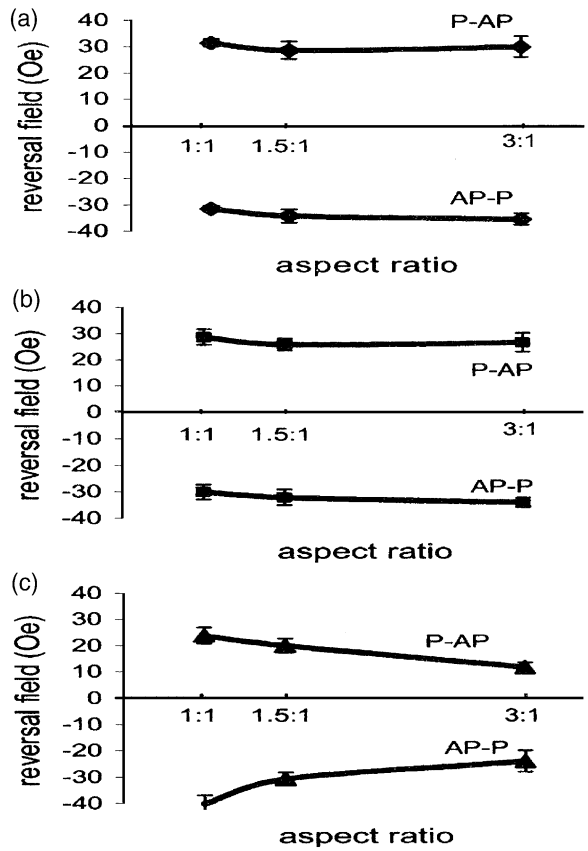

Fig. 24. Switching fields for MRAM tunnel junctions, comprising of a multiplayer of Ta/NiFe/MnFe/NiFe/Al_2O_3/NiFeCo as a function of device aspect ratio for three different widths: a) 0.7 μm, b) 1 μm and c) 2 μm after Warot et al. [104]. P-AP represents the parallel to antiparallel switching field, AP-P represents the antiparallel to parallel switching field.

Nozaki and Matsuyama [105] have considered size dependence of switching current and energy barrier in the magnetization reversal of MRAM cells. To do this they investigated rectangular cell shapes. The switching current I and the energy barrier ΔE show strong dependence on width w and thickness t of the cells as indicated in Fig. 25. I was found to be proportional to t/w, while ΔE was proportional to wt^2. A sufficient energy barrier against thermal activation is essential in the practical applications of these materials to MRAM. This

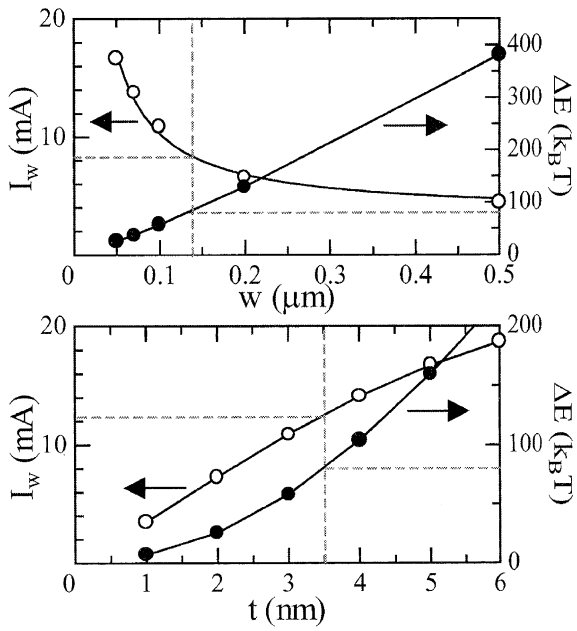

Fig. 25. Calculated variation of switching current I_w and energy barrier ΔE with width w and thickness t of a perrmalloy MRAM cell after Nozaki and Matsuyama [105].

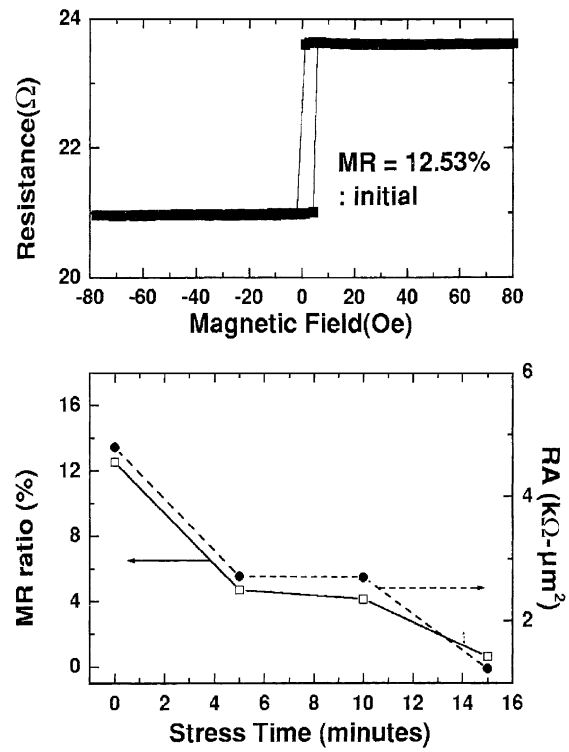

Fig. 26. Magnetoresistance curve of a 200 μm^2 tunnel junction (upper figure) and variation of magnetoresistance (MR) and resistance area product (RA) with time at a constant applied voltage of 0.75 V showing the progress in electrical breakdown (lower figure) after Kim et al. [106].

amounts to $\Delta E > 80\ k_B T$. Larger values of t are needed because w is being reduced to increase data storage density. However larger values of t also increase the switching current, which is undesirable. Optimization of aspect ratio of the cell resulted in length to width ratio of $l/w \sim 1.5$ and a width of $w \sim 0.1$ μm which gave a data density of 5 Gbit/sq.in (0.8 Gbit/cm^2), for thermal stability a thickness of $t > 3.5$ nm was needed.

Junction reliability is related to the electrical breakdown mechanism. Kim et al. [106] studied the electrical breakdown in tunnel junctions and how this depended on the area of the junction. A "constant voltage stress" was applied to tunnel junctions with cross sectional areas of 200 μm^2 and 0.5 μm^2. The mechanism of the electrical breakdown appeared to be quite different depending on the area of the junction. For large area junctions the MR decreased gradually with time, as shown in Fig. 26, while for small area junctions the MR decreased abruptly with time. The breakdown voltage was found to be a function of the junction barrier thickness. Higher breakdown voltages were found for thicker barriers, and for smaller cross sectional areas. The breakdown voltage also depended on the barrier layer oxidation time, which relates to the junction barrier quality. Time needed for electrical breakdown to occur under constant voltage stress was found to be shorter for larger area junctions, because the process is dependent on defects such as pinholes, process induced defects and side wall damage, all of which increase with area. For small area junctions no change seemed to occur in MR prior to electrical breakdown.

Low resistance tunnel junctions of a few Ω μm^2 are needed for read head sensor applications. Wang et al. [107] have investigated different materials for continuous thin barriers in order to produce low resistance spin dependent tunnel junctions as

shown in Fig. 27. However with thinner barrier layers the probability of "pinholes" increases and their presence in the insulating layer degrades the performance of tunnel junctions, including the tunneling magnetoresistance. Various different oxide barriers were studied, including HfO_x, $HfAlO_x$, $ZrAlO_x$ and AlO_x. It was found that HfO_x made the thinnest continuous insulating barriers. A resistance area product of 0.4 $\Omega\ \mu m^2$ was obtained with a 0.4 nm HfO_x barrier with 5.5% tunneling magnetoresistance. A resistance area product of 0.65 $\Omega\ \mu m^2$ was obtained with a 0.2 nm *Hf* + 0.3 nm AlO_x barrier with 9% tunneling magnetoresistance.

Neel ("orange peel") coupling between thin films is caused by magnetostatic interactions across the interface arising from free poles generated on the surface when it is corrugated. Surface roughness together with high magnetization in the surface layer is the root cause of Neel coupling. This is undesirable in magnetic tunnel junctions because there is a shift, known as the bias field, in the response of the free layer to an applied magnetic field. Particularly in the case of low field devices and applications it is highly desirable to reduce or eliminate Neel coupling. Wang et al. [108] have looked at spin dependent tunnel junctions with a new structure for the pinned layer giving reduced Neel coupling between the free and pinned layers. They used a five layer modified synthetic antiferromagnetic composite as the pinned electrode, with three layers of ferromagnet and two intermediate layers of ruthenium. The new structure that has been developed gives a strong antiferromagnetic coupling between the magnetic layers in the composite pinned electrode. This antiparallel magnetization configuration is maintained under normal operating conditions of the tunnel junction. The net bulk magnetic moment of the composite pinned electrode is thereby kept close to zero to minimize the coupling even in the presence of surface roughness. The new structure reduced the bias field to less than 80 A/m (1 Oe) as shown in Fig. 28.

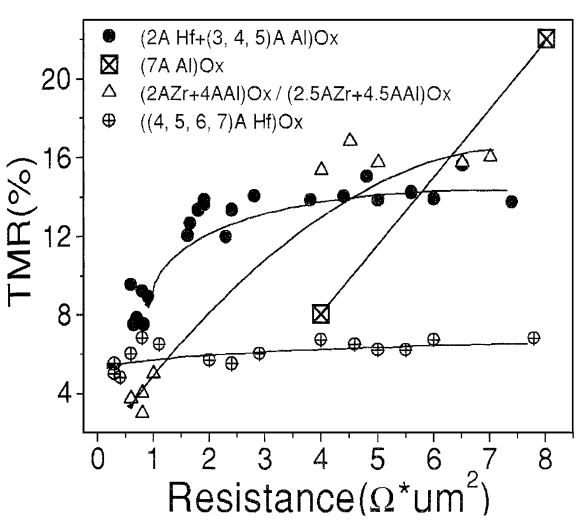

Fig. 27. Tunnel magnetoresistance and resistance area product for tunnel junctions constructed with different barrier layer materials, after Wang et al. [107].

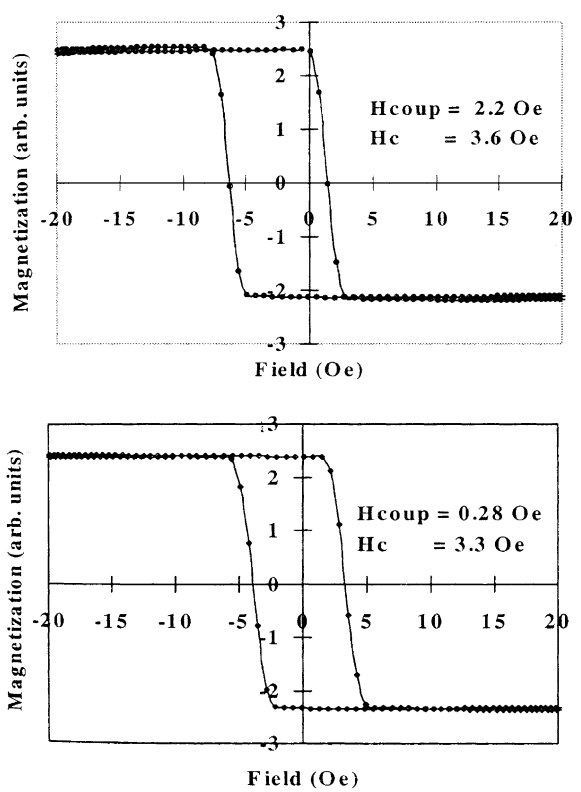

Fig. 28. Magnetic hysteresis loop for magnetic tunnel junction using conventional structure (upper figure) and for the new modified synthetic antiferromagnet composite pinned layer (lower figure). This shows the reduction in the bias or offset field due to reduction in Neel coupling, after Wang et al. [108].

5.2.3. Nanoscale magnetic switching materials

Future high density recording media applications with data storage densities in the range of 10^{12} bits/sq.in will require the development of materials for nanoscale magnetic switching structures. Nanodots in the single domain state with well controlled anisotropy and low hysteresis have potential for i) high resolution field sensors and ii) high density low power magnetic logic gates. Multi domain structures are undesirable from the viewpoint of data storage, but the formation of multidomains is suppressed in very small structures, which is therefore doubly advantageous. Cowburn [109] formed nanometer scale magnets which have different magnetic properties from the bulk magnets formed of the parent bulk material. These nanoscale magnets exhibit suppression of multidomain configurations and configurational anisotropy.

Configurational anisotropy is a form of anisotropy that arises from the details of the magnetic moment configuration in a small structure. This anisotropy is the difference in energies between states with different deviations of the magnetic moment configuration from complete uniformity. It is different from shape anisotropy, but has some similar characteristics. For example the energy of perfectly uniformly magnetized square is independent of the direction of magnetization, but immediately the non-uniformity of magnetization is allowed energy differences arise between the different directions of magnetization. It was found that the competition between exchange and demagnetizing energy is the determining factor in deciding the actual magnetic moment configuration in these nanostructures, and slight differences in these configurations can lead to very different dependence of magnetization on applied field Therefore attention has to be given to geometry, even at these small scales, in order to obtain the desired magnetic moment configuration.

Fidler et al. [110] have modeled fast switching behavior in square nanoelements $10 \times 10 \times 1$ nm, both with and without anisotropy. The modeling of switching dynamics of these structures was performed using a combination of finite element modeling and micromagnetic Landau-Lifschitz-Gilbert modeling. Switching time and critical field were found to depend strongly on the Gilbert damping parameter and the field sweep rate. All other factors being equal the longest switching times were found in the elements with uniaxial anisotropy, while the shortest switching times were in material without anisotropy.

Schrefl et al. [111] have modeled coercivity and remanence in annealed and monodisperse self assembled nanoparticles of FePt. These "as synthesized" particles have a disordered fcc structure. Heat treatment can cause a phase transformation at 530 °C which results in an ordered face centered tetragonal structure with high anisotropy of typically 10^6 J/m^3 and a coercivity that can reach 716 kA/m. Model calculations were made using a modified Stoner-Wolfarth model (to allow for interactions between the particles) and these results were compared with a combined finite element model together with a Landau-Lifschitz-Gilbert micromagnetic calculation. It was found that remanence enhancement occurred only when the exchange interaction was reduced, as indicated in Fig. 29, in contrast to the usual result where remanence increased with exchange interaction.

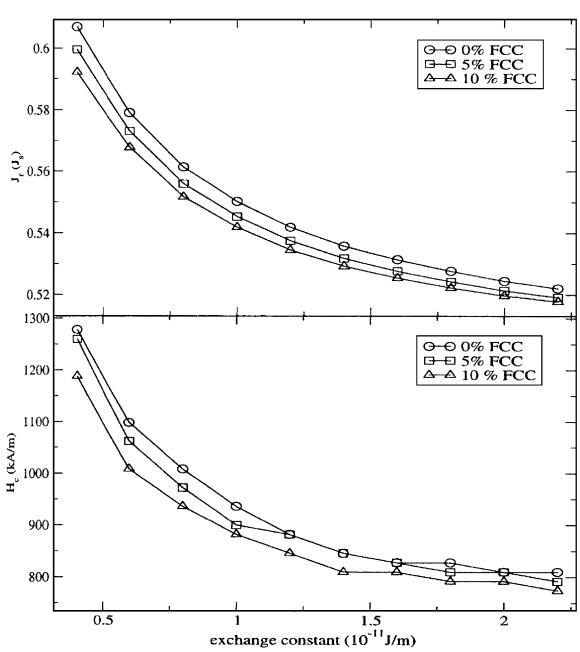

Fig. 29. Calculated variation of reduced remanence (ratio of remanence to saturation) and coercivity of FePt nanoparticle assemblies with exchange interaction for different volume fractions of the disordered fcc phase after Schrefl et al. [111].

6. Conclusions

In recent years there has been an explosion of interest in new magnetic materials. These materials provide a fertile subject area for scientific investigations which transcend the boundaries of condensed matter physics, materials science and electrical and computer engineering. They also have current and future technological applications in diverse areas such as energy conversion devices, field generation, sensors, actuators, data storage and memory devices.

In this review recent scientific and technological advances have been described in four important categories of magnetic materials that are currently of high interest. These include: soft magnets, hard magnets, magnetomechanical and magnetoelectronic materials. It is seen that the requirements in each of these areas are quite different and yet there is also much common ground, so that an understanding of one of these groups of materials inevitable leads to a better understanding of the other groups. Although the range of magnetic materials will continue to diversify in the future the same basic concepts described here will remain essential to the understanding and future development of magnetic materials.

Improvements and completely new developments in the various types of magnetic materials have been highlighted through the consideration of a few selected new magnetic materials which are at the leading edge of current research and development, including: amorphous magnetic fibers, nanocrystalline permanent magnet materials, ferromagnetic shape memory alloys and spintronic materials. For each type of material the various magnetic properties of prime interest have been discussed and how these properties can be controlled and improved. In most cases it can be seen that in the future the greatest progress is likely to being made through emphasis on control of the materials on the smallest scale that is possible. Currently this emphasis is on “nanostructured” materials. The interesting result is that the boundary between engineering applications and fundamental science is beginning to be erased as the two fields of activity meet on the scale of nanostructured materials. For the development of better magnetic materials in the future, the emphasis will shift down to an even smaller scale.

Acknowledgements

This was supported by the US Department of Energy, Office of Basic Energy Sciences, Materials Sciences Division. Ames Laboratory is operated by Iowa State University for the US Department of Energy under Contract No.W-7405-ENG-82.

References

[1] Chikazumi S. Physics of ferromagnetism., 2nd Ed. Oxford: Clarendon Press, 1997.
[2] Jiles D. Introduction to magnetism and magnetic materials., 2nd Ed. London & New York: Chapman and Hall, 1998.
[3] Yoshizawa Y, Oguma S. Yamauchi K. J Appl Phys 64;6044:1988.
[4] Herzer G. J Mag Mag Mater 157;133:1996.
[5] Hernando A, Navarro I, Gorria P. Phys Rev B51;3281:1995.
[6] Hernando A, Kulik T. Phys Rev B49;7064:1994.
[7] Ohnaka I, Fukusako T, Ohmichi T, et al., Proceedings of the fourth conference on rapidly quenched metals, 1982, p. 31.
[8] Mohri K, Humphrey F.B., Yamosaki J, Okamura K. IEEE Trans Mag 1984;20:1409.
[9] Mohri K, Humphrey FB, Kawashima K, et al. IEEE Trans Mag 1990;26:1789.
[10] Atkinson D, Squire PT, Gibbs MRJ, Hogsdon SN. J Phys D (Appl Phys) 1994;27:1354.
[11] Mohri K, Uchiyama T, Shen LP, Cai CM, Panina LV, Honkura Y, Yamamoto M. IEEE Trans Mag 2002;38:3063.
[12] Panina LV, Mohri K. Appl Phys Lett 1994;65:1189.
[13] Chiriac H, Neagu M, Vazquez M, Hristoforou E. J Mag Mag Mater 2002;242:251.
[14] Chiriac H, Neagu M, Hison C. IEEE Trans Mag 2002;38:2823.
[15] Chiriac H, Ovari TA. IEEE Trans Mag 2002;38:3057.
[16] Zhukova V, Chizhik A, Zhukov A, Torcunov A, Larin V, Gonzalez J. IEEE Trans Mag 2002;38:3090.
[17] Betancourt I, Valenzuela R, Vazquez M. J Appl Phys 2003;93:8110.
[18] Ciureanu P, Melo LGC, Yelon A. J Mag Mag Mater 2002;242:224.
[19] Li YF, Vazquez M, Chen DX. IEEE Trans Mag 2002;38:3096.
[20] Zhukova V, Zhukov A, Blanco JM, Gonzalez J, Gomez-Polo C, Vazquez M. J Appl Phys 2003;93:7208.

[21] Losin C, Gomez-Polo C, Knobel M, Grishin A. IEEE Trans MAG 2002;38:3087.
[22] Zhukov A. J Mag Mag Mater 2002;242:216.
[23] Kulik T, Wlazlowska A, Ferenc J, Latuch J. IEEE Trans Mag 2002;38:3075.
[24] Fert A, Piraux L. J Mag Mag Mater 1999;200:338.
[25] Petzold J. J Mag Mag Mater 2002;242:84.
[26] Himeno A, Ono T, Nasu S, Shigeto K, Mibu K, Shinjo T. J Appl Phys 2003;93:8430.
[27] Moulin J, Champion Y, Varga LK, Greneche JM, Mazaleyrat F. IEEE Trans MAG 2002;38:3015.
[28] Parker RJ. Advances in permanent magnets. New York: Wiley, 1990.
[29] Rodewald W, Wall B, Katter M, Uestuener K, Steinmetz S. In: Hadjipanayis GC, editor. Proceedings of the 17th International Workshop on rare earth magnets and their applications, Newark, Delaware. Princeton, New Jersey: Rinton Press; 2002, p. 25.
[30] Walmer MH. In Hadjipanayis GC, editor. Proceedings of the 17th International workshop on rare earth magnets and their applications, Newark, Delaware. Princeton, New Jersey: Rinton Press; 2002, p. 37.
[31] Kronmuller H. In: Hadjipanayis GC, editor. Proceedings of the 17th International workshop on rare earth magnets and their applications, Newark, Delaware. Princeton, New Jersey: Rinton Press; 2002, p. 804.
[32] Gutfleisch O. J Phys D Appl Phys 2000;33:R157.
[33] Gutfleisch O, Khlopkov K, Eckert D, Wall B, Rodewald W, Hinz D, Muller KH. In: Hadjipanayis GC, editor. Proceedings of the 17th International workshop on rare earth magnets and their applications, Newark, Delaware. Princeton, New Jersey: Rinton Press; 2002, p. 566.
[34] Kneller EF, Hawig R. IEEE Trans Mag 1991;27:3588.
[35] Withanawasam L, Hadjipanayis GC, Krause FR. J Appl Phys 1994;75:6646.
[36] Hadjipanayis GC, Withanawasam L, Krause RF, IEEE Trans Mag 1995;31:3596.
[37] Davies HA. J Mag Mag Mater 1996;157:11.
[38] Ding J, McCormick PG, Street R. JMMM 1993;124:1.
[39] Schrefl T. Phys Rev 1994;B496:100.
[40] Hadjipanayis GC. J Mag Mag Mater 1999;200:373.
[41] Stamps RL. J Mag Mag Mater 2002;242:139.
[42] Skomski R, Kashyap A, Qiang Y, Sellmyer DJ. J Appl Phys 2003;93:6477.
[43] Gutfleisch O, Bollero A, Handstein A, Hinz D, Kirchner A, Yan A, Muller KH, Schultz L. J Mag Mag Mater 2002;242:1277.
[44] Chiriac H, Lupu N, Greneche JM. J Mag Mag Mater 2002;242:1311.
[45] Rodewald W, Wall B, Katter M, Uestuener K. IEEE Trans Mag 2002;38:2955.
[46] Wang ZC, Davies HA, Harland CL. IEEE Trans Mag 2002;38:2967.
[47] Zhou J, Skomski R, Sellmyer DJ. J Appl Phys 2003;93:6495.
[48] Betancourt I, Valenzuela R. J Appl Phys 2003;93:6933.
[49] Branagan DJ, Meacham BE, McCallum RW, Dennis KW, Kramer MJ. J Appl Phys 2003;93:7969.
[50] Wang H, Zhang Y, Jin ZQ, Hadjipanayis GC. J Appl Phys 2003;93:7978.
[51] Ono H, Tayu T, Waki N, Sugiyama T, Shimada M, Kanou M, Yamamoto H, Takasugi K. J Appl Phys 2003;93:8113.
[52] Huang Y, Zhang Y, Hadjipanayis GC, Simopoulos A, Weller D. IEEE Trans Mag 2002;38:2604.
[53] Barmak K, Kim J, Ristau RA, Lewis LH. IEEE Trans Mag 2002;38:2799.
[54] Crew DC, Stamps RL. J Appl Phys 2002;93:6483.
[55] Zhou J, Skomski R, Li X, Tang W, Hadjipanayis GC, Sellmyer DJ, IEEE Trans Mag 2002;38:2802.
[56] Thang PD, Bruck E, Tichelaar FD, Buschow KHJ, de Boer FR. IEEE Trans Mag 2002;38:2934.
[57] Huang YH, Zhang Y, Hadjipanayis GC. J Appl Phys 2003;93:7172.
[58] Ding Y, Yamamuro S, Farrell D, Majetich SA. J Appl Phys 2003;93:7411.
[59] Simizu S, Obermyer RT, Zande B, Chandhok VK, Margolin A, Sankar SG. J Appl Phys 2003;93:8134.
[60] Cullity BD. Fundamentals of magnetostriction. Journal of Metals 1971;23:35.
[61] Clark AE. Magnetostrictive rare earth iron compounds. In: Wohlfarth EP, editor. Ferromagnetic materials, vol. 1. Amsterdam: North Holland Publishing; 1980. p. 1–2.
[62] Jiles DC. Development and characterization of the highly magnetostrictive alloy Tb-Dy-Fe for use in sensors and actuators. In: New Materials and their applications. Bristol: Institute of Physics Publishing; 1990.
[63] Schieber MM. Experimental magnetochemistry. New York: John Wiley & Sons, 1967.
[64] Jiles DC, Atherton DL, J Phys D (Appl Phys) 1984;17:1265.
[65] Jiles DC. J Phys D (Appl Phys) 1995;28:1537.
[66] Li L, Jiles DC. J Appl Phys 2003;93:8480.
[67] Calkins FT, Smith RC, Flatau AB. IEEE Trans Mag 2000;36:429.
[68] Dapino MJ, Smith RC, Flatau AB, IEEE Trans Mag 2000;36:545.
[69] Ullakko K, Huang JK, Kantner C, O'Handley RC, Kokorin VV. Appl Phys Lett 1996;69:1966.
[70] Vassiliev A. J Mag Mag Mater 2002;242:66.
[71] Sozinov A, Likhachev A, Ullakko K. IEEE Trans Mag 2002;38:2814.
[72] Pasquale M, Sasso CP, Besseghini S, Villa E, Lograsso TA, Schlagel DL. IEEE Trans Mag 2002;38:2847.
[73] Khovailo VV, Oikawa K, Abe T, Takagi T. J Appl Phys 2003;93:8483.
[74] Samolyuk GD, Antropov VP. J Appl Phys 2003;93:6882.
[75] Casanova F, Batlle X, Labarta A, Marcos J, Manosa L, Planes A. J Appl Phys 2003;93:8313.
[76] Han MG, Jiles DC, Snyder JE, Lo CCH, Leib JS, Paulsen JA, Pecharsky AO. Appl Phys 2003;93:8486.
[77] Han M, Paulsen JA, Snyder JE, Jiles DC, Lograsso TA, Schlagel DL. IEEE Trans Mag 2002;38:3252.

[78] Jiles DC, Lee SJ, Han M, Lo CCH, Snyder JE, Gschneidner KA, Pecharsky VK, Pecharsky AO, Lograsso TA, Schlagel DL, J Magnetics 2003;8:1.
[79] Han M, Jiles DC, Lee SJ, Snyder JE, Lograsso TA, Schlagel DL. Angular dependence of the unsual first order transition temperature in $Gd_5(Si_xGe_{1-x})_4$, Presented at the International Magnetics Conference, Boston, Massachusetts, March 30–April 3, 2003. IEEE Transactions on Magnetics 2003;39(November) (in press).
[80] Clark AE, Hathaway KB, Wun-Fogle M, Restorff JB, Lograsso TA, Keppens VM, Petculescu G, Taylor RA. J Appl Phys 2003;93:8621.
[81] Cheng SF, Das BN, Wun-Fogle M, Lubitz P, Clark AE. IEEE Trans Mag 2002;38:2838.
[82] Kellogg R, Flatau AB, Clark AE, WunFogle M, Lograsso TA. J Appl Phys 2003;93:8495.
[83] Johnson M. IEEE Spectrum 2000;37(2):33.
[84] Kryder MH. MRS Bulletin 1996;21(9):17.
[85] Baibich MN, Broto JM, Fert A, Nguyen F, Petroff F, Etienne P, Creuzet G, Frederick A, Chazelas J. Phys Rev Letts 1988;61:2472.
[86] Sauerenback F, Barnas J, Binasch G, Vohl M, Gruenberg P, Zinn W. Thin Solid Films 1989;175:317.
[87] Takahata T, Arakai S, Shinjo T. J Mag Mag Mater 1989;82:287.
[88] Parkin SSP, Bhadra R, Roche KP. PhYS Rev Lett 1991;66:2152.
[89] White RL. IEEE Trans MAG 1992;28:2842.
[90] Fert A, Gruenberg P, Barthelmy P, et al. J Mag Mag Mater 1995;140:1.
[91] Leib JS, Baker BJ, Shen YP, Snyder JE, Kawaguchi T, Jiles DC. IEEE Trans Mag 2003;39(5) (in press).
[92] Brug JA, Anthony TC, Nickel JH. MRS Bulletin 1996;21(9):23.
[93] Bass J, Pratt WP. J Mag Mag Mater 1999;200:274.
[94] Jedema FJ, Filip AT, van Wees BJ. Nature 2001;410:345.
[95] Schumacher HW, Chappert C, Crozat P, Sousa RC, Freitas PP, Miltat J, Ferre J. IEEE Trans Mag 2002;38:2480.
[96] Veloso A, Freitas PP, Wei P, Barradas NP, Soares JC, Almeida B, Sousa JB. Appl Phys Lett 2000;77:1020.
[97] Ventura JO, Sousa JB, Salguiero da Silva MA, Freitas PP, Veloso A. J Appl Phys 2003;93:7690.
[98] Yuasa H, Fukuzawa H, Iwasaki H, Yoshikawa M, Takagishi M, Sahashi M. J Appl Phys 2003;93:7915.
[99] Moodera JS, Kinder LR, Wong TM, Meservey R. Phys Rev Lett 1995;74:3273.
[100] Moodera JS, Mathon G. J Mag Mag Mater 1999;200:248.
[101] Zhu JG. J Appl Phys 2000;87:6668.
[102] Anil Kumar PS, Lodder JC. J Phys D (Appl Phys) 2000;33:2911.
[103] Reiss G, Brueckl H, Thomas A, Justus M, Meyners D, Koop H. J Magnetics (Korea) 2003;8:24.
[104] Warot B, Petford-Long AK, Anthony TC. J Appl Phys 2003;93:7287.
[105] Nozaki Y. Matsuyama K. J Appl Phys 2003;93:7295.
[106] Kim KS, Cho BK, Kim TW, Park WJ. J Appl Phys 2003;93:8364.
[107] Wang J, Liu Y, Freitas PP, Snoeck E, Martins JL, J Appl Phys 2003;93:8367.
[108] Wang D, Daughton JM, Qian Z, Nordman C, Tondra M, Pohm AV. J Appl Phys 2003;93:8558.
[109] Cowburn RP. J Mag Mag Mater 2002;224:505.
[110] Fidler J, Schrefl T, Tsiantos VD, Forster H, Dittrich R, Suess D. IEEE Trans Mag 2002;38:2520.
[111] Schrefl T, Hrkac G, Suess D, Scholz W, Fidler J. J Appl Phys 2003;93:7041.